HIGH RESOLUTION LASER SPECTROSCOPY OF CESIUM AND RUBIDIUM MOLECULES WITH OPTICALLY INDUCED COHERENCE

A Dissertation

by

HUI CHEN

Submitted to the Office of Graduate Studies of
Texas A&M University
in partial fulfillment of the requirements for the degree of

DOCTOR OF PHILOSOPHY

August 2006

Major Subject: Physics

HIGH RESOLUTION LASER SPECTROSCOPY OF CESIUM AND RUBIDIUM MOLECULES WITH OPTICALLY INDUCED COHERENCE

A Dissertation

by

HUI CHEN

Submitted to the Office of Graduate Studies of
Texas A&M University
in partial fulfillment of the requirements for the degree of

DOCTOR OF PHILOSOPHY

Approved by:

Co-Chairs of Committee,	Marlan O. Scully
	M. Suhail Zubairy
Committee Members,	George R. Welch
	Vladimir A. Sautenkov
	Goong Chen
Head of Department,	Edward Fry

August 2006

Major Subject: Physics

ABSTRACT

High Resolution Laser Spectroscopy of Cesium and Rubidium Molecules with Optically Induced Coherence. (August 2006)

Hui Chen, B.S.; M.S., University of Science and Technology of China;

M.S., Texas A&M University

Co–Chairs of Advisory Committee: Dr. Marlan O. Scully
Dr. M. Suhail Zubairy

This work is devoted to the study of the quantum coherent effects in diatomic molecular systems by using high resolution laser spectroscopy. In particular, we have studied the rubidium diatomic molecular gaseous medium's absorption spectrum with high resolution single mode laser spectroscopy. The derived electronic and rotational vibrational constants were used in the backward Raman amplification experiment of Rb diatomic molecule. Both experimental results and theoretical calculation confirms that there is strong backward directionally dependent radiation. This effect can further be utilized in remote detection of chemical material.

In the saturated spectroscopy experiment of the cesium diatomic molecule, long-lived ground state coherence was observed. The coherence would decay at a rate less than the natural life time of the excited states, which indicates great possibility for performing the quantum optics experiments previously performed in atomic systems only.

Electromagnetically induced transparency has been observed in many atomic systems for many years, while it has been seldom realized in molecular systems. In our experiment of electromagnetically induced transparency in cesium diatomic molecules, we utilized Λ energy levels, and observed subnatural linewidth. This is

the first time to realize a Λ type EIT in a molecular ensemble. This experiment will lead to many other experiments of quantum effects in a molecular system, such like magnetic optical rotation, light storage in ensemble of molecules.

Magnetically induced chirality in an atomic ensemble is also investigated in my research.

ACKNOWLEDGMENTS

First of all I would like to thank Dr. Marlan O. Scully and Dr. M. Suhail Zubairy for their direction and encouragement.

Dr. Vladimir A. Sautenkov and Dr. Yuri V. Rostovtsev have given me the most important help in my research and writing the dissertation. Without them this work would never have been possible. Special thanks are due to Dr. George R. Welch for enormous encouragement. I would like to thank Dr. Goong Chen and Dr. Philips Hemmer for many helpful and stimulating discussions.

I would like to thank Dr. Edward Fry, Dr. A. L. Ford, Dr. R. Kenefick for their kind advice and encouragements.

I would also like to gratefully acknowledge useful discussions with Aihua Zhang, Paul Hsu, Hebin Li as well as support of the Welch Foundation, the Office of Naval Research, and the Texas Advanced Research and Technology Program.

Finally, I would like to thank my parents and family for their inspiration and support.

TABLE OF CONTENTS

CHAPTER Page

LIST OF FIGURES

FIGURE Page

FIGURE Page

CHAPTER I

INTRODUCTION

A. Motivation

The macroscopic coherence in the interaction of light and matter reveals the quantum nature of the world. On the other hand, besides its philosophical general meaning, coherent preparation is a method that produces remarkable changes in the optical properties of a gas phase atomic or molecular medium that has enormous number of applications.

Laser induced coherence of the atomic or molecular energy states causes the modification of optical response of the medium. This coherence leads to quantum interference between the excitation alternative that allows one to pathways which control the optical response. Therefore electromagnetic fields provide a method to manipulate the properties of matter such as absorption, dispersion and a variety of nonlinear characteristics.

A coherent light allows one to go beyond the natural limit and get high resolution spectroscopy and other unconventional phenomenons such like Raman gain, electromagnetically induced transparency, nonlinear magnetic optical rotation. The enhanced nonlinearity can also bring the light pulse to slow down dramatically therefore useful to quantum information storage.

Chirality has been observed in the crystal with magnetic field and in the solution of organic molecule. The idea that quantum coherent effect can enhance the chiral effect in medium was proposed by several researcher. We investigated the effect in the rubidium atom.

The journal model is Physical Review A.

B. Optically induced coherent effects

Quantum coherence in atomic and molecular physics has led to many exciting and surprising results [1]. In the last several decades, many experiments and theoretical works plotted the subtle picture of quantum mechanical nature of atom and molecule. Among them, coherent effects played important roles.

Hanle effect [2] probably was the first light-matter interaction,which clearly demonstrated the coherence between atomic levels played an important role. linear polarized light excites the ensemble of atoms in a week magnetic field, the polarization of fluorescence will evolve under the influence of the magnetic field.

Laser was invented in the 1960s. Its invention greatly enhanced the research of quantum coherence and nonlinear spectroscopy. A lot of experiments were conducted in the 60 and 70's. Among them, interaction between two level atoms/molecule with single mode electromagnetic radiation are the most fundamental and subtle. The splitting of a level under strong optical field was firstly described by Autler and Townes [3]. Interference between decay processes was discovered by Fano [4]. Mollow predicted three-peak spectrum of resonance fluorescence [5] and experimentally demonstrated by several groups.

The more generalized models involve multilevel atom interacting with several single mode field, which reveals more unexpected nature. Coherent population trapping was investigated by researchers in Pisa. Coherent superposition of the atomic ground states causes the absorption of resonant field dramatically decreased. This effect be explained with dark state and bright state.

Stimulated Raman Adiabatic Passage (STIRAP) using the adiabatically turn-on and turn-off pulses can transfer atom from one ground state to another one and therefore manipulate state population and create maximum coherence [6].

Quantum interference between two upper states introduced by a strong pump field, will turn an opaque medium for probe laser into a transparent one [7]. The optical property such as absorption and transmission spectrum of a medium could be significantly modified by the effects of atomic/molecular coherence under the interaction between coherent radiation field and quantized system. Near electromagnetically induced transparency resonance, the dispersion is so huge and the absorption is nearly zero that people use EIT to reduce the speed of light to nearly zero and even negative.

Since the group speed of the light in the EIT medium is very small, people can achieve light storage in such conditions, which will be very important to the quantum communication.

1. Physics

The most fundamental aspects in the interaction of atom-field is a two level atom coupled with a single mode electromagnetic field. Within dipole approximation and rotating wave approximation interaction of a single atom with a single-mode field can be solved exactly.

We can write the wave function of a two level atom as

$$|\psi(t)\rangle = C_a(t)|a\rangle + C_b(t)|b\rangle, \tag{1.1}$$

where C_a and C_b are the probability amplitude of finding the atom in the states $|a\rangle$ and$|b\rangle$. The Schrödinger equation is

$$|\dot{\psi}(t)\rangle = -\frac{i}{\hbar}\mathscr{H}|\psi(t)\rangle, \tag{1.2}$$

with

$$\mathscr{H} = \mathscr{H}_0 + \mathscr{H}_1. \tag{1.3}$$

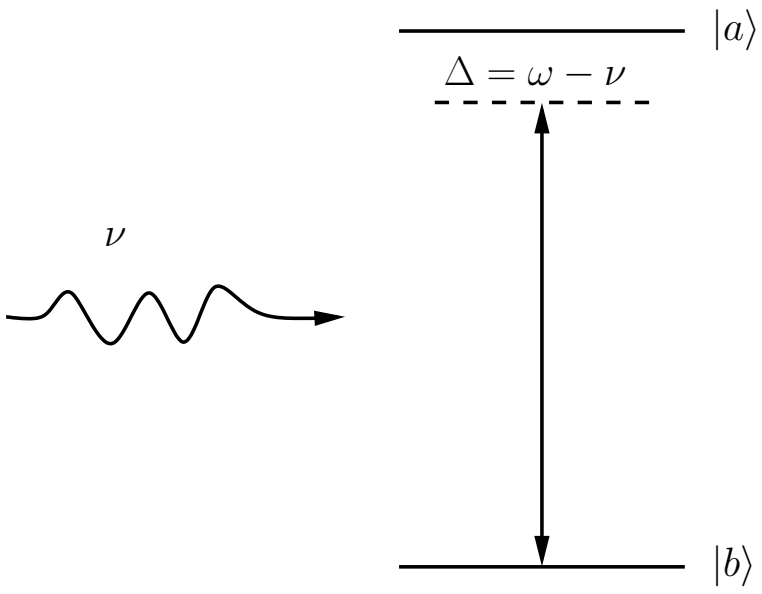

Fig. 1. Two-level atom interacting with a single mode field

The Hamiltonian for a free atom $\mathscr{H}_0$ can be write as

$$\mathscr{H}_0 = \hbar\omega_a|a\rangle\langle a| + \hbar\omega_b|b\rangle\langle b|; \tag{1.4}$$

The interaction hamiltonian $\mathscr{H}_1 = -e\mathbf{r}\cdot\mathbf{E}(r_0,t)$ is given by

$$\begin{aligned}\mathscr{H}_1 &= -e(|a\rangle\langle a| + |b\rangle\langle b|)x(|a\rangle\langle a| + |b\rangle\langle b|)E(z,t) \\ &= -(\wp_{ab}|a\rangle\langle b| + \wp_{ba}|b\rangle\langle a|)E(t);\end{aligned} \tag{1.5}$$

$\wp_{ab} = \wp^*_{ba} = e\langle a|x|b\rangle$ is the electric dipole moment matrix element. Solving the schrödinger equation, along with initial conditions, we can determine the evolution of atom under the influence of the single mode field.

2. CPT, dark and bright states

Coherent superposition of atomic states leads to many novel effects such like coherent population trapping. In this effect the the atom is prepared in a coherent superposition of the ground states, it will keep in this state and will not jump to the upper state, therefore no absorption or fluorescence emission will be observed.

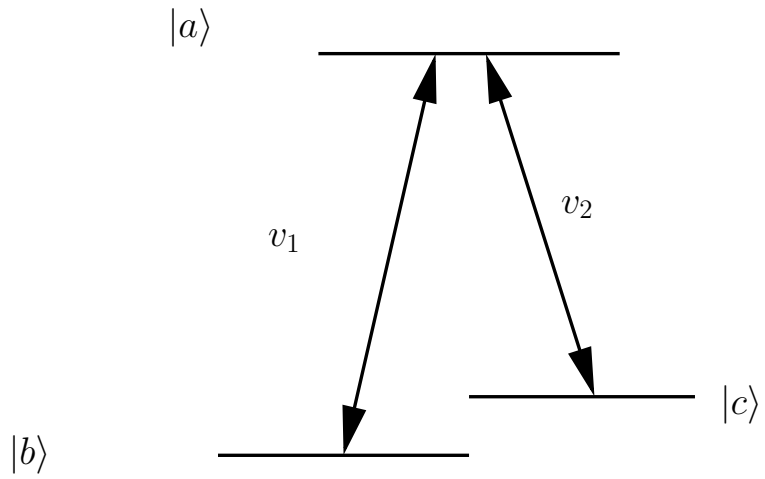

Fig. 2. Λ configuration of three level atom. Two laser fields with frequency ν_1 and ν_2 coupling three levels $|a\rangle$,$|b\rangle$ and $|c\rangle$

The Hamiltonian for a three level atom can be written as

$$\mathscr{H} = \mathscr{H}_0 + \mathscr{H}_1, \tag{1.6}$$

where,

$$\mathscr{H}_0 = \hbar\omega_a|a\rangle\langle a| + \hbar\omega_b|b\rangle\langle b| + \hbar\omega_c|c\rangle\langle c| \tag{1.7}$$

$$\mathscr{H}_1 = -\frac{\hbar}{2}(\Omega_{R1}e^{-i\phi_1}e^{-i\nu_1 t}|a\rangle\langle b| + \Omega_{R2}e^{-i\phi_2}e^{-i\nu_2 t}|a\rangle\langle c|) + H.c. \tag{1.8}$$

($\Omega_{R1}e^{-i\phi_1}$ and $\Omega_{R2}e^{-i\phi_2}$ are Rabi frequency of the pump and probe fields, which are equal to $\wp_{ab}\mathscr{E}/\hbar$ and $\wp_{ac}\mathscr{E}/\hbar$. The atomic wave function can be written as

$$|\psi(t)\rangle = c_a(t)e^{-i\omega_a t}|a\rangle + c_b(t)e^{-i\omega_b t}|b\rangle + c_c(t)e^{-i\omega_c t}|c\rangle. \tag{1.9}$$

The equation of motion of the atom wave function can be derived from solving the Schrödinger equation $i\hbar|\dot{\psi}\rangle = \mathscr{H}|\psi\rangle$,assume the laser fields are on resonance,

$$\dot{c}_a = \frac{i}{2}(\Omega_{R1}e^{-i\phi_1}c_b + \Omega_{R2}e^{-i\phi_2}c_c) \tag{1.10}$$

$$\dot{c}_b = \frac{i}{2}\Omega_{R1}e^{i\phi_1}c_a \tag{1.11}$$

$$\dot{c}_c = \frac{i}{2}\Omega_{R2}e^{i\phi_2}c_a \tag{1.12}$$

it can be easily shown that if the atom in the state

$$|\psi(t)\rangle = \frac{\Omega_{R2}e^{-i\phi_2}|b\rangle - \Omega_{R1}e^{-i\phi_1}|c\rangle}{\sqrt{\Omega_{R1}^2 + \Omega_{R2}^2}} \tag{1.13}$$

We can find that $|\dot{\psi}(t)\rangle = 0$, it means that the population is trapped in the lower states and there is no absorption even we have another field present. This is due to destructive interference between the two transitions in this three level atom.

The bright state is

$$|\psi(t)\rangle = \frac{\Omega_{R1}e^{-i\phi_1}|b\rangle + \Omega_{R1}e^{-i\phi_1}|c\rangle}{\sqrt{\Omega_{R1}^2 + \Omega_{R2}^2}} \tag{1.14}$$

As shown in Fig. 3, only the bright state will interact with the incident light field, if the atom is prepared in the dark state, it will not interact with light. If both fields are pulses, by carefully designing the time difference of the pulses, the population transferring from one state to another state can be achieved. The technique is called stimulated Raman adiabatic passage(STIRAP). The STIRAP technique can be used to create maximum coherence for atoms and molecules [8, 6].

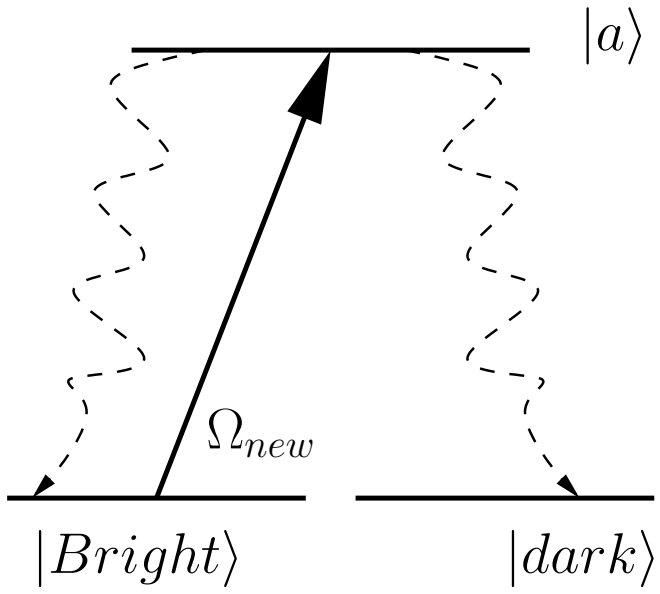

Fig. 3. Bright state and dark state interaction with field, $\Omega_{new} = \sqrt{\Omega_1^2 + \Omega_2^2}$

3. Electromagnetically induced transparency

For a three level and two coupling fields system, there could be three kinds of configuration, (Λ, V, or cascade configuration). If one field is very strong, it can introduce interference between two levels, the other field(probe), will have much less absorption, the medium for it become effectively transparent.

For example, in the Λ system, we can write the Hamiltonian as,

$$\mathscr{H} = \hbar\omega_a|a\rangle\langle a| + \hbar\omega_b|b\rangle\langle b| + \hbar\omega_c|c\rangle\langle c| + -\frac{\hbar}{2}\left(\frac{\wp_{ab}\mathscr{E}}{\hbar}e^{-i\nu t}|a\rangle\langle b| + \Omega_\mu e^{-i\phi_\mu}e^{-i\nu_\mu t}|a\rangle\langle c|\right) + H.c. \tag{1.15}$$

Solving the density matrix equation of motion,

$$\dot{\rho} = -\frac{i}{\hbar}[\mathscr{H}, \rho] - \frac{1}{2}\{\Gamma, \rho\} \tag{1.16}$$

we get the off diagonal density matrix element as,

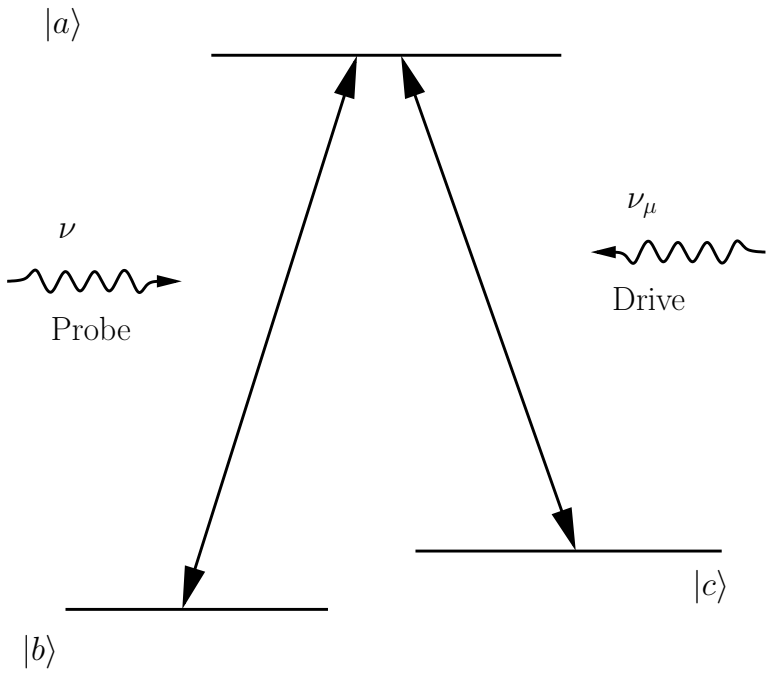

Fig. 4. Electromagnetically induced transparency in Λ configuration. Three-level atom interacting with two fields of frequencies of ν and ν_p

$$\rho_{ab}(t) = \frac{i\wp_{ab}\mathcal{E}e^{-i\nu t}(\gamma_3 + i\Delta)}{2\hbar[(\gamma_1 + i\Delta)(\gamma_3 + i\Delta) + \Omega_\mu^2/4]} \tag{1.17}$$

The real and imaginary parts of the complex susceptibility $\chi = \chi' + i\chi''$ are given below:

$$\chi' = \frac{N_a|\wp_{ab}|^2\Delta}{\epsilon_0\hbar Z}[\gamma_3(\gamma_1 + \gamma_3) + (\Delta^2 - \gamma_1\gamma_3 - \Omega_{mu}^2/4)] \tag{1.18}$$

$$\chi'' = \frac{N_a|\wp_{ab}|^2}{\epsilon_0\hbar Z}[\Delta^2(\gamma_1 + \gamma_3) - \gamma_3(\Delta^2 - \gamma_1\gamma_3 - \Omega_{mu}^2/4)] \tag{1.19}$$

N_a is the atomic number density,

$$Z = (\Delta^2 - \gamma_1\gamma_3\Omega_{mu}^2/4)^2 + \Delta^2(\gamma_1 + \gamma_3)^2 \tag{1.20}$$

In figure 5, we can see at the ω_0, the reduced absorption can be achieved.

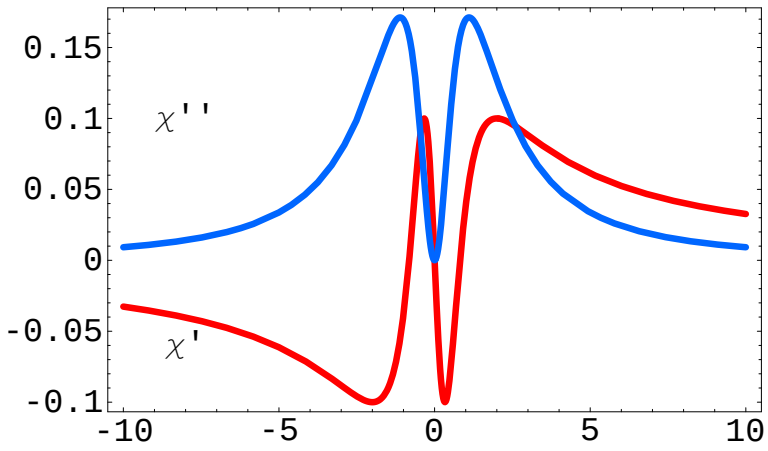

Fig. 5. Absorption and dispersion curve near atomic resonance

4. Slow light

Group velocity dispersion relation is

$$v_g = \frac{d\omega}{dk} = \frac{c}{n(\omega) + \omega \frac{dn(\omega)}{d(\omega)}}. \tag{1.21}$$

Near the atomic transition, dispersion is big but the absorption is also huge. but with the help of electromagnetically induced transparency, the absorption is close to zero while the dispersion is even sharper. George Welch achieved the very slow of speed of light in HOT rubidium vapor cell as low as 90m/sec [9].

5. Dark polariton and light storage

Due to the slow group velocity of light in the EIT medium, the light pulse gets compressed in the medium. The atoms are driven into a coherent superposition of ground states or sublevels of ground state. M.D. Lukin named them as dark polariton

state. Switching off the control field will effectively stop the probe light pulse and the information of probe pulse field will be stored in the atomic medium. The coupling laser is turned back on at a later time and the probe pulse is regenerated. The quantum information is read out from the quantum memory device then.

This idea will have application in the quantum information processing and quantum communication.

6. Chirality

The terrestrial life can only utilize the L-enantiomers of of amino acids, which is known as 'homochirality of life'. In searching the origin of the phenomenon, scientists investigated the chirality in the photochemical reactions. The external influence of circularly polarized light was found causing the chirality of the reaction. Natural optical activity in the media lacking mirror symmetry can cause the polarization rotation of light, while the magnetic optical activity can also has the same effect. Scientists were trying to connect magnetic effect to enantioselectivity in chemical reaction. Recently, magnetically induced chiral effects experimentally verified magnetically induced chirality was reported in the complex ion [10].

Agarwal proposed new idea about create magnetochiral effect in the media under the influence of a coherent control field that is resonant or close to resonance to an appropriate atomic transition [11]. Vladamir Sautenkov experimentally demonstrated this effect in 2004 [12].

7. Raman scattering

Raman spectroscopy is a powerful tool to investigate the molecular vibrational and rotational transitions. Raman spectroscopy was brought to practically importance by the invention of laser.

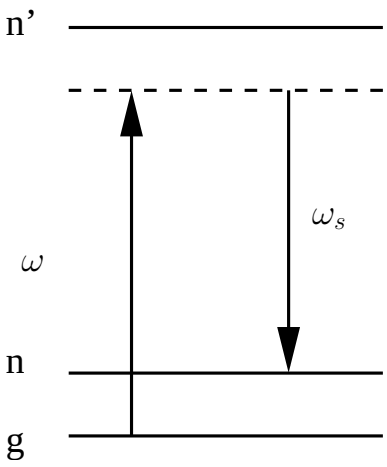

Fig. 6. Raman process that generates Stokes field ω_s

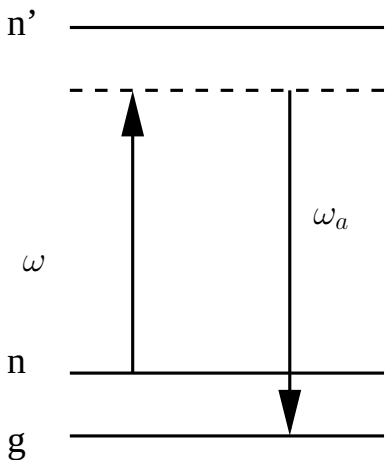

Fig. 7. Raman process that generates anti-Stokes field ω_{as}

a. Spontaneous Raman scattering

Spontaneous Raman scattering is typically very weak, and as a result the main difficulty of Raman spectroscopy is separating the weak inelastically scattered light from the intense Rayleigh scattered laser light.

b. Stimulated Raman scattering

If the pump laser intensity is large, an appreciable fraction of the molecules will be excited into the final state and the intensity of Raman scattered light will be correspondingly large.

c. Coherent anti-Stokes Raman spectroscopy

Coherent anti-Stokes Raman spectroscopy (CARS) use two lasers. The frequency of two lasers ω_1, ω_2 are chosen that $\omega_1 - \omega_2 = \omega_v$. here the ω_v is the vibrational or rotational energy been investigated. New Stokes and anti-Stokes waves are generated from nonlinear interaction. as in Fig. 8, the ω_1 and ω_2 excited molecule to the

Raman-active level, these excited molecules then interact with incident light ω_1 and generate anti-Stokes wave $\omega_a = 2\omega_1 - \omega_2$. CARS is call four-wave parametric mixing process since there are four waves involved in generating the anti-Stokes wave.

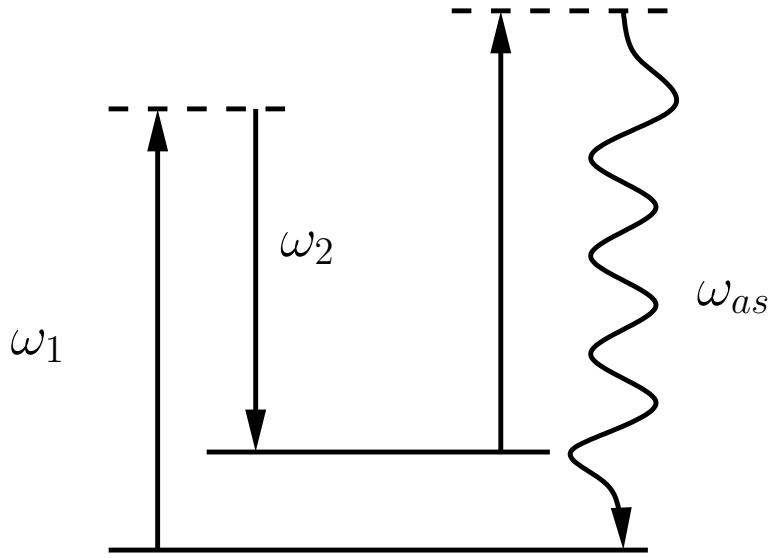

Fig. 8. Level diagram of coherent anti-Stokes Raman spectroscopy

C. Laser spectroscopy

The basic knowledge of the structure of atom-molecule has been obtained from optical spectroscopy. Information about molecular structure and the interaction with their surroundings may be derived in many measures from the absorption or emission spectra.

Wavelength of spectra lines can determine the energy of different levels of atomic or molecular system. The line intensity can give the transition probability. The natural linewidth can determine the lifetimes of the excited states. The Doppler width will give the velocity distribution. Pressure broadening gives the information

about collision process and the intermolecular potential. The Zeeman splitting give the magnetic moments. The hyperfine splitting yields information about the interaction between the nuclei and the electrons. Femtosecond spectroscopy can give the dynamics about molecular association and dissociation.

Many spectroscopic instruments helped to bring this technology into the new era. But laser re-invented the whole area since its debutante. Not only its intensity but also the coherent property of the electromagnetic radiation gives rise of many new spectroscopy technology.

1. Doppler free spectroscopy

As our knowledge of spectroscopy got deeper, the limit of the line broadening become essential. Among several reasons of broadening, Doppler broadening is usually the dominant contribution. to the observed width of lines.

The moving atom with the quantum transition frequency ω_0 will have an effective frequency

$$\omega = \omega_0 - kv, \tag{1.22}$$

Since the thermal distribution of atoms obeys Maxwell distribution,

$$f(v)dv = \sqrt{\frac{M}{\pi 2k_B T}} \exp(-\frac{Mv^2}{2k_B T})dv, \tag{1.23}$$

we find that the absorption has the Gaussian line shape fucntion

$$g_D(\omega) = \frac{c}{u\omega_0\sqrt{\pi}} \exp\{-\frac{c^2}{u^2}(\frac{\omega - \omega_0}{\omega_0})^2\} \tag{1.24}$$

The Doppler broadening line has a full width at half maximum

$$\frac{\Delta\omega_D}{\omega_0} = 2\sqrt{\ln 2}\frac{u}{c} \tag{1.25}$$

There are several methods to overcome this Doppler broadening, crossed atom or molecule beam with light beam, the saturated absorption spectroscopy and two photon spectroscopy.

a. Saturated absorption spectroscopy

This method use an intense pump laser beam to reduce the population difference between two levels as atoms are excited to the upper level. It is also called as hole burning. The hole burnt has a width

$$\Delta\omega_{hole} = \Gamma\left(1 + \frac{I}{I_{sat}}\right)^{1/2}. \tag{1.26}$$

As in Fig. 9, The pump and probe beams are in opposite directions, so they have opposite k. They will interact with different atoms with different velocity, only when the velocity of the atoms are zero, the pump beam with change the population difference for the probe beam and thereafter a Doppler free peak will appear on the absorption line of the probe beam.

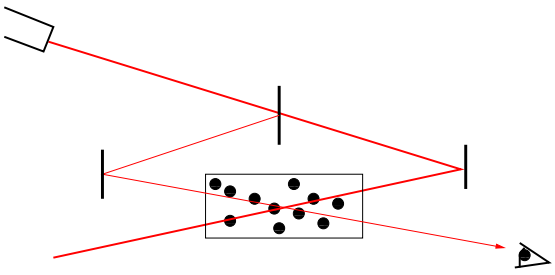

Fig. 9. Saturated absorption spectroscopy experiment

There are several ways to overcome the Doppler broaden effect, like saturation spectroscopy, polarization spectroscopy, two-photon spectroscopy and molecular beam technology.

D. Goal

The main objectives of my research are to:

- To study the Rubidium diatomic molecule spectrum, energy levels and potential of the ground state and first electronic excited state using laser spectroscopy and laser induced fluorescence spectroscopy, to experimentally demonstrate the backward Raman amplification.
- To investigate the ground coherence of Cesium Molecule using saturation spectroscopy , to design and experimentally explore electromagnetically induced transparency in Cesium molecular gaseous medium.
- To study the magnetically induced chirality in Rubidium medium under EIT condition.

CHAPTER II

SPECTROSCOPY OF RUBIDIUM DIMER

A. High resolution optical spectrum of rubidium diatomic molecule

1. Introduction

Alkali molecular spectroscopy, which has been studied intensively for years, is very important for fundamental physics and applications [13, 14, 15]. In the last thirty years, laser methods have greatly improved molecular spectroscopic techniques [16, 17, 18]. In particular, laser-induced fluorescence has become a powerful method to probe the energy levels of atoms and molecules. Recent improvements in tunable diode lasers have given us a very efficient spectroscopic tool, with resolution that may be limited only by laser linewidth [19].

One application is the use of alkali diatomic molecules as a medium for high-power tunable lasers. Lasing in Na_2, Bi_2 and Te_2 bands has already been observed [20]. Another possible application derives from quantum coherence effects in these molecules [21].

In this paper, we describe our experiments on absorption and fluorescence spectra within the transition band $A^1\Pi_u \rightarrow X^1\Sigma_g^+$ of rubidium molecules in the wavelength range 640–740 nm.

2. The experiment

Our experimental setup is shown in Fig. 10. A tunable free-running single-mode diode laser (Sanyo DL4039-011) is used for spectroscopy of rubidium molecules. The temperature of the diode laser is regulated by a Peltier junction driven by a temperature controller. The laser wavelength is set coarsely by adjusting the temperature

(+0.3 nm/K). Fine frequency tuning is performed by variation of injection current (-0.1 cm^{-1}/mA). The laser is tunable over a range of about 20 GHz without mode hopping.

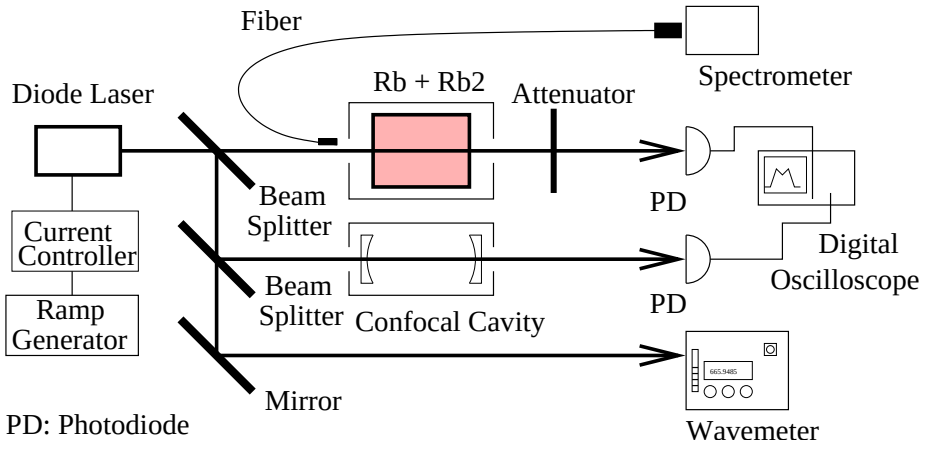

Fig. 10. Rubidium diatomic molecular spectroscopy: experimental setup

We use an all-sapphire cell [22] of length $l = 15$ cm in an oven heated to the range of 500°K–600°K. The cell contains a natural isotopic mixture of rubidium metal. Three thermocouples placed at the ends and center point of the cell are used to monitor the temperature of the rubidium vapor. At high temperature, when the vapor pressure is greater than 0.01 Torr, the saturated rubidium vapor is a mixture of atoms and diatomic molecules due to atomic collisions. A large percentage of total rubidium atoms will form rubidium diatomic molecules.

Transmission spectra of rubidium molecules at different cell temperatures are shown in Fig. 11. Transmission of white light through rubidium vapor is measured by a diffraction spectrometer Ocean Optics HR2000 (spectral resolution 0.065 nm). We start to observe absorption signal when the temperature of the cell reaches 450°K.

At this temperature, the density of rubidium atoms is 2.1×10^{14} cm^{-3}. When the temperature reaches 515°K, the density of rubidium atoms is 3.4×10^{15} cm^{-3}, the absorption can reach as much as 60%. If we raise the temperature above 550°K, the absorption in the center of the vibrational band is saturated (meaning that practically all light at these wavelengths is absorbed). The absorption spectra appear as gaussian shaped envelopes with a small modulation, which reflects transitions between different vibrational sublevels of ground and first excited electronic states of the rubidium molecule.

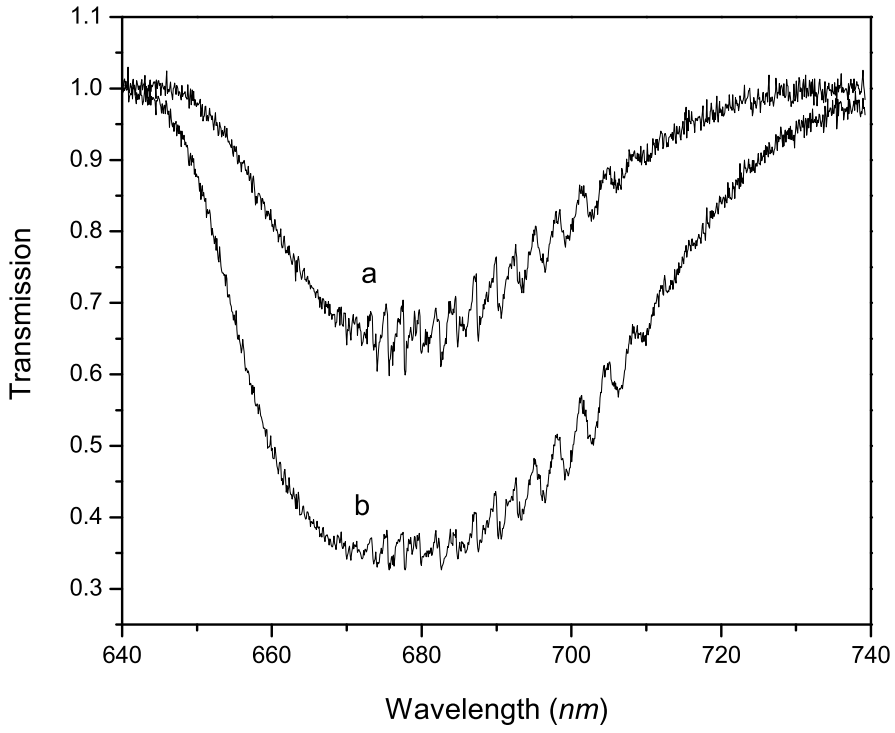

Fig. 11. Transmission of white light through Rb_2 molecules at different temperatures: $T_a = 483$°K, $T_b = 512$°K.

In order to resolve transitions between rotational sublevels a tunable diode laser is used. The laser beam power is reduced to avoid non-linear effects. The collimated laser beam is propagated through the rubidium cell and then detected by a photodiode. Part of the laser beam before the cell is sent to a reference confocal cavity with free spectral range 1.5 GHz. Signals from photodiodes are recorded on a digital oscilloscope. When the laser wavelength is fixed, it can be measured with accuracy ± 0.0002 nm by a Burleigh wavemeter WA-1500.

3. Results

The transmission spectra for different wavelengths (667 nm and 666 nm) are presented in Figs. 12 and 13. Molecules in the ground state absorb a photon, jump to the next electronic state $A^1\Pi_u^+$, then decay to many vibrational sublevels in the ground electronic states. From fluorescence spectra, we find that only specific ground vibrational sublevel can be pumped. In our experiments, vibrational quantum number of the initial $X^1\Sigma_g^+$ state that can be pumped is 6. Rotational spectral components are well resolved in these two figures. The resolution of spectra is near 0.001 cm^{-1}, which is limited by laser linewidth. Using the separations of these rotational absorption peaks, we can estimate the rotational constant for the ground state, $B = 0.020$ cm^{-1}. This value is in good agreement with previously published data [15, 23].

We have chosen several different laser frequencies for study. After tuning the laser to the desired wavelength (within the Doppler width), we then obtain fluorescence spectra from the molecules being pumped by the laser. Fig. 12 and 13 show absorption spectra for two different narrow spectral regions. In each of these regions, one sees various rotational and hyperfine components. The two regions differ by approximately 1 nm and correspond to different vibrational transitions. In the first region, we have chosen two different rotational components, marked by arrows in the figure, and in

the second region we have marked three different peaks. For each of these 5 peaks, the wavelength of the laser has been accurately measured with a wavemeter.

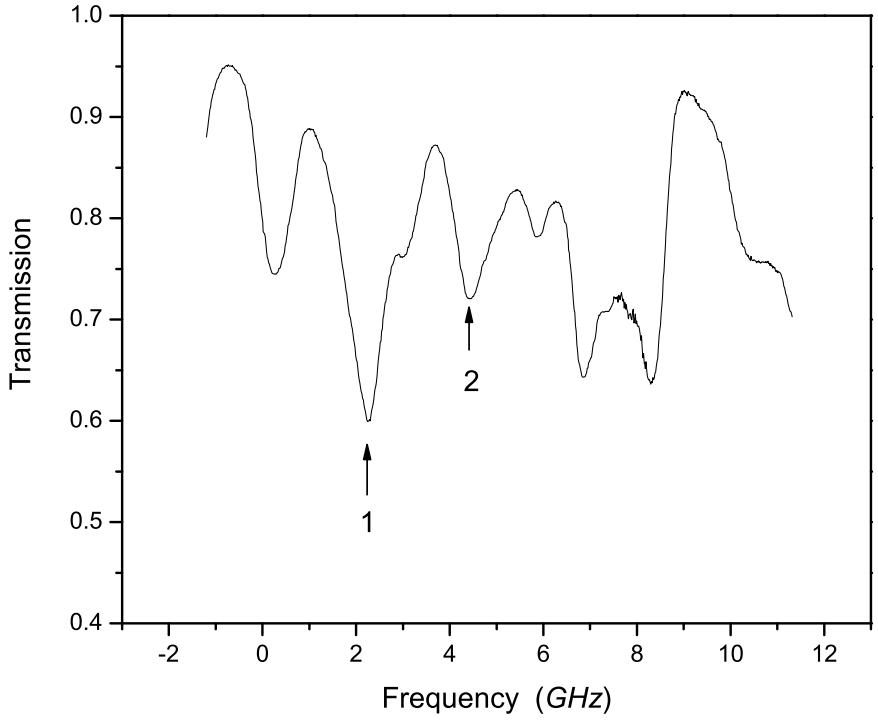

Fig. 12. Rotational transmission spectrum at wavelength $\lambda = 667$ nm. The spectral components labelled 1 and 2 have wavelengths $\lambda_1 = 666.9485(2)$ nm and $\lambda_2 = 666.9455(2)$ nm

For each of the chosen wavelengths we have measured the laser-induced fluorescence spectra. A small part of the backward fluorescence is collected with an optical fiber and analyzed wth a diffraction spectrometer. The results are shown in Figs. 14 and 15. Vibrational spectral components are very well resolved in laser-induced fluorescence spectra and the laser populates only one rotational sublevel of

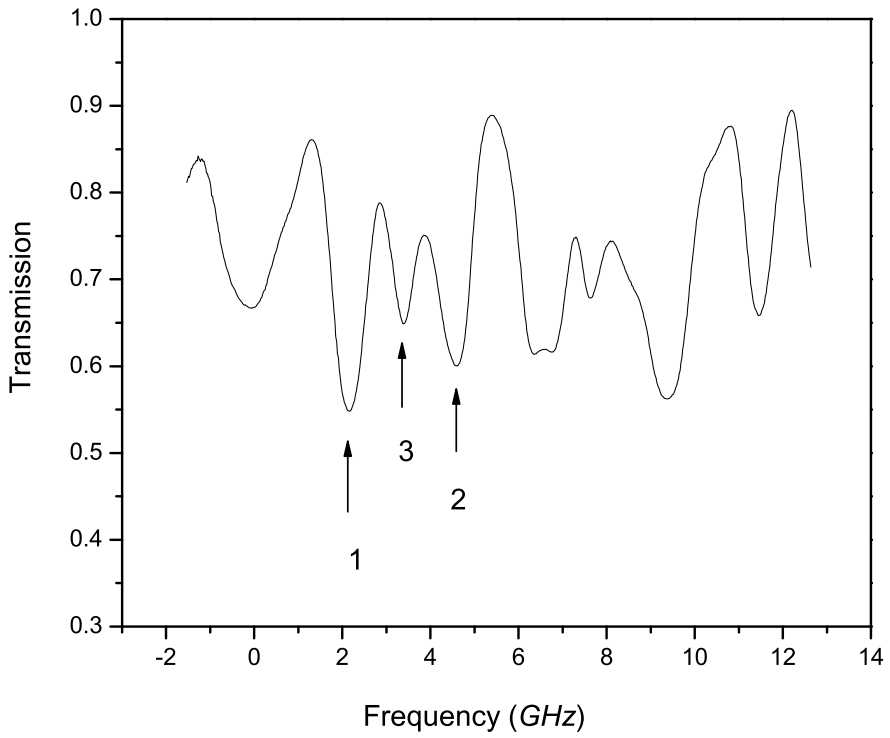

Fig. 13. Rotational transmission spectrum at wavelength $\lambda = 666$ nm. The spectral components labelled 1, 2, and 3 have wavelengths $\lambda_1 = 665.9800(2)$ nm, $\lambda_2 = 665.9761(2)$ nm and $\lambda_3 = 665.9780(2)$ nm

the vibrational excited level. Then the population decays to different vibrational sublevels of the ground electronic state according to the Frank-Condon principle and produces different spectral components in the fluorescence. These components are well resolved. From Ref. [23] we know that for each level

$$E = T_e + \omega_e(\nu + \frac{1}{2}) - \omega_e x_e(\nu + \frac{1}{2})^2 \tag{2.1}$$

so, the transition energy T is given by:

$$T = T_e + \omega'_e(\nu' + \frac{1}{2}) - \omega'_e x'_e(\nu' + \frac{1}{2})^2 \\ -[\omega''_e(\nu'' + \frac{1}{2}) - \omega''_e x''_e(\nu'' + \frac{1}{2})^2] \tag{2.2}$$

The vibrational splitting of the ground state is obtained by fitting of the spectra and a polynomial approximation of the peaks positions. We find $\omega''_e = 57.58$ cm^{-1} and $\omega''_e x''_e = 0.15$ cm^{-1}, which are in good agreement with Ref. [15].

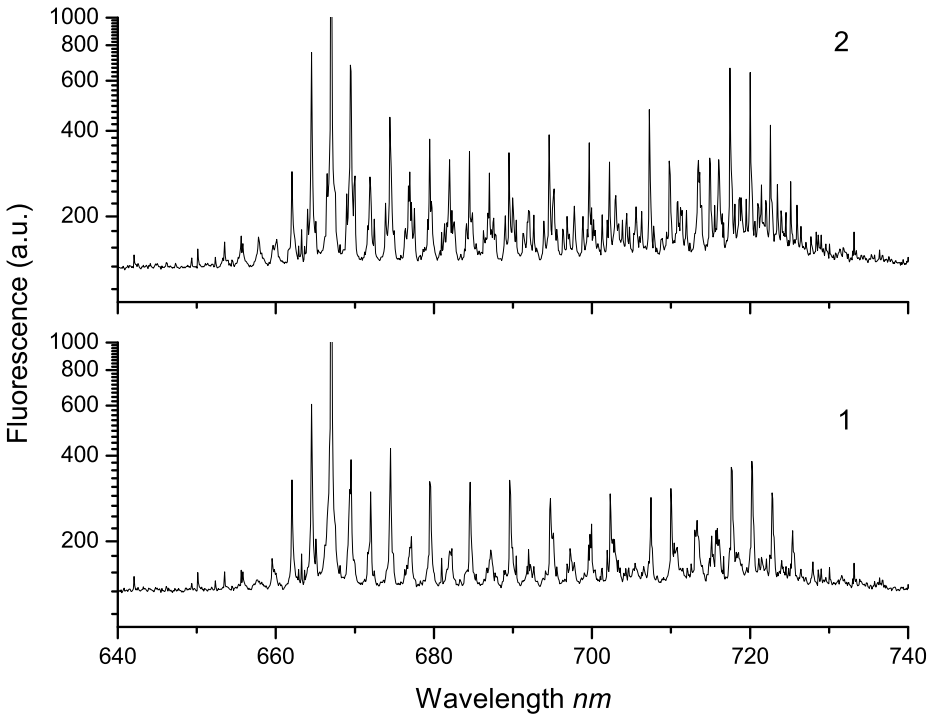

Fig. 14. Fluorescence spectrums of Rb_2 induced by laser excitation at the wavelengths 1 and 2, marked in Fig. 12

One of the interesting aspects of these fluorescence spectra that there are fluorescence lines on the red side (above 720 nm) where the absorption of the rubidium

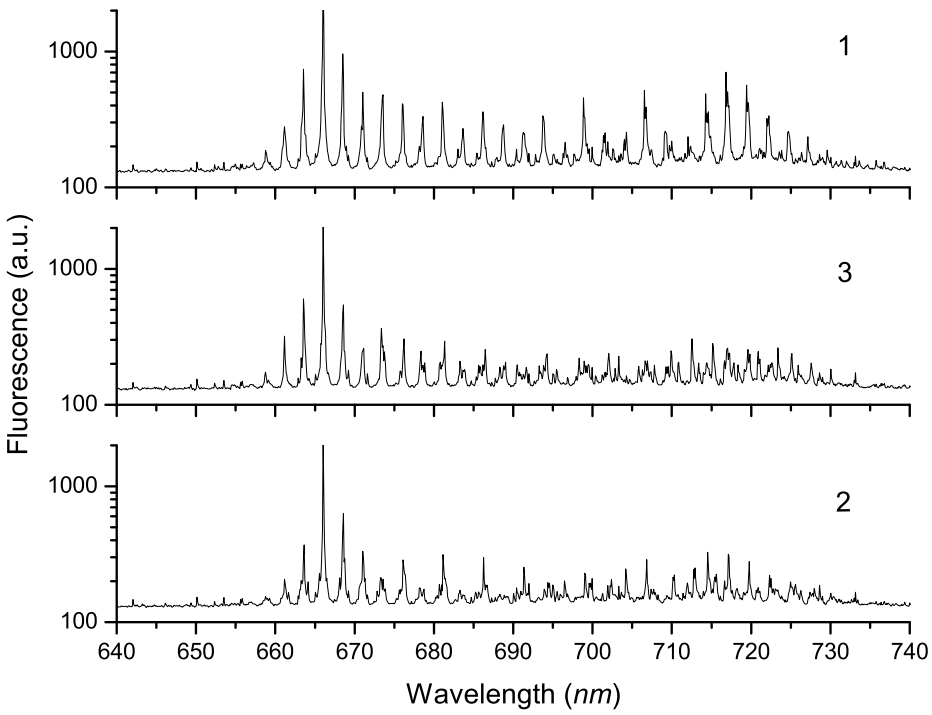

Fig. 15. Fluorescence spectrums of Rb_2 induced by laser excitation at the wavelengths 1,2 and 3, marked in Fig. 13.

molecules is relatively small. This could provide a way to build up a rubidium molecular laser system similar to optically pumped sodium, Te_2, and Bi_2 molecular lasers [24]. To realize this, one has to reach high enough optical pump intensity to create population inversion and gain on these transitions. Coupling between vibrational modes can be studied by using 2D coherent femtosecond spectroscopy [25].

Another interesting point is that the rubidium molecule has the potential for realization of many coherence effects in a molecular system, such as electromagnetically induced transparency (EIT), Stimulated Raman Adiabatic Passage (STIRAP) and Femtosecond Adaptive Spectroscopic Techniques Coherent anti-Stokes Raman

Spectroscopy (FAST CARS).

4. Conclusions

We have measured well-resolved rotational spectral components in rubidium diatomic molecules using a tunable diode laser. Wavelengths of several rotational components were measured with good accuracy using a wavemeter. The vibrational structure of the ground state is well resolved by the laser-induced fluorescence technique. Fluorescence is observed in the red wing of the band where molecular absorption is small. This indicates that an optically pumped rubidium molecular laser may be realized in these spectral regions.

With the knowledge of the transmission and fluorescence spectra, further study of many coherent effects in Rubidium diatomic molecules, such as EIT, STIRAP and FAST CARS may be possible.

B. Backward Raman amplification in rubidium molecules

1. Introduction

The continuous monitoring of the atmosphere for traces of various gases and biopathogens at parts-per-million (ppm) concentrations and distances of the order of 1–10 km is a challenging problem with applications from the control of environmental pollution to national security [26]. However, in order to continuously scan the 2π sector of the sky, new technology is needed. Recently a new approach (Stand-Off Superradiant (SOS) spectroscopy) to improve LIDAR performance has been suggested [27].

There are several implementations of SOS. The first detection scenario of SOS has two logical steps. In the first step, Raman or two photon pumping of the gas molecules from the ground state to an appropriate excited state takes place. The

excitation is achieved via simultaneous action of two synchronized picosecond laser pulses with a difference frequency that is resonant with the ground to the vibrationally excited state energy difference, or a sum frequency being resonant with the ground to the electronically excited state energy difference. Then, in the second step, strong emission in the backward direction is generated via swept-gain superradiance (see Refs. [28, 29] and references therein).

The second implementation is based on the Raman gain in a molecular medium [30, 31, 32]. One sends a train of pulses, and a pulse is amplified in the backward direction. The selectivity of the method is determined by resonance with the vibrational frequencies or the electronic transition of molecules.

Both these schemes have the potential for a real-time detection of poison gases (e.g., $COCl_2$) and atmospheric pollutants (e.g., NO). The essential advantage of this scheme is that the signal intensity exceeds the backscattering signal intensity of the usual LIDAR schemes by many orders of magnitude.

In this paper, we have experimentally demonstrated backward Raman gain in Rb diatomic molecules vapor within the transition band $A^1\Pi_u \rightarrow X^1\Sigma_g^+$ of rubidium molecules in the wavelength range 640–740 nm and performed simulations to support our experimental results. The motivation of our research is to demonstrate an experimental possibility to implement and study a system exhibiting swept gain. We show that molecular diatomic molecules can be used for this purpose, as they are formed under reasonable experimental conditions available in the laboratory [33]. The spectroscopic properties of the diatomic molecules are known; alkali molecules have been studied intensively for years, their parameters are very important for fundamental physics and applications [34, 14, 15, 16, 17, 18, 19]. Such information allows us to perform simulations to explain experimental results.

The structure of the paper is the following. In the next section we describe the

experimental setup has been used. Then, we discuss the obtained results and present simulations that supports the observed results.

2. Experimental setup

The experimental setup is shown in Fig. 16. A tunable free-running single-mode diode laser is used for observation and study backscattering from rubidium molecules. The laser wavelength is set coarsely by adjusting the temperature (+0.3 nm/K). The temperature of the diode laser is regulated by a Peltier junction driven by a temperature controller. Fine frequency tuning is performed by variation of injection current (-0.1 cm^{-1}/mA). The laser is tunable over a range of about 20 GHz without mode hopping. Laser emission radiation is collimated into parallel beam with diameter of 0.12 cm.

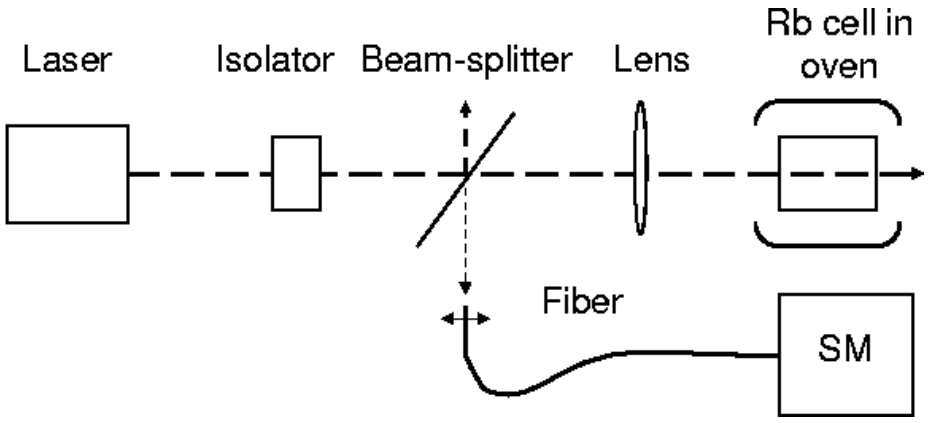

Fig. 16. Experimental setup for backward Raman amplification

The cell contains a natural isotopic mixture of rubidium metal. Three thermocouples placed at the ends and in the center point of the cell are used to monitor the temperature of the rubidium vapor. We use an all-sapphire cell [22] of length $l = 15$ cm in an oven heated to the range of 500°K–600°K. At higher temperatures,

when the vapor pressure is greater than 0.01 Torr, the saturated rubidium vapor is a mixture of atoms and diatomic molecules formed via atomic collisions.

Transmission spectra of rubidium molecules at different cell temperatures are shown in Fig. 11. Transmission of white light through rubidium vapor is measured by a diffraction spectrometer Ocean Optics HR2000 (spectral resolution 0.065 nm). We observe absorption signal when the temperature of the cell higher than 450°K. If we raise the temperature above 550°K, the absorption in the center of the vibrational band is saturated (meaning that practically all light at these wavelengths is absorbed).

The experimental condition to study the backward Raman amplification are the following. We focus the laser beam (power of 8 mW) by a lens (f = 15 cm) into a spot of 0.015 cm of a cell with a rubidium vapor. The temperature of the cell is 493 K. At this temperature, the pressure of rubidium molecules is 2 10^{-4} Torr. Under these conditions, the emission measured in backward direction consists of two parts: well collimated amplified Raman scattering and diffuse scattered radiation. The scattered light collected by the lens and send to a beam-splitter. Spatial dependence of scattered emission spectra is analyzed by the diffraction spectrometer (SM) with a fiber input. The fiber is installed at xy translation stage.

3. Results and discussion

The absorption spectra are shown in Fig. 11 for two different temperatures. Rb_2 diatomic molecule molecule in the ground state ($X^1\Sigma_g^+$) absorbs a photon to get excited to the electronic state $A^1\Pi_u^+$ see schematic level structure of Rb_2 shown in 29, then decay to many vibrational sublevels in the ground state. Because the vibrational energy for Rb_2 is much smaller than kT, the population is distributed by thermal motion among vibrational levels of the ground state, and hence there are many absorption lines originated from the ground state.

In the current experiments, we drive the Rb_2 molecular system with relatively strong CW laser field (we use a lens to focus the laser beam from the diode laser into the Rb cell, see Fig. 16) and measure scattered radiation in the backward direction. We have chosen for study a laser frequency that corresponds to $\lambda = 667$ nm. The frequency of observed lines correspond to two-photon transitions between vibrational states of ground state, $X^1\Sigma_g^+$.

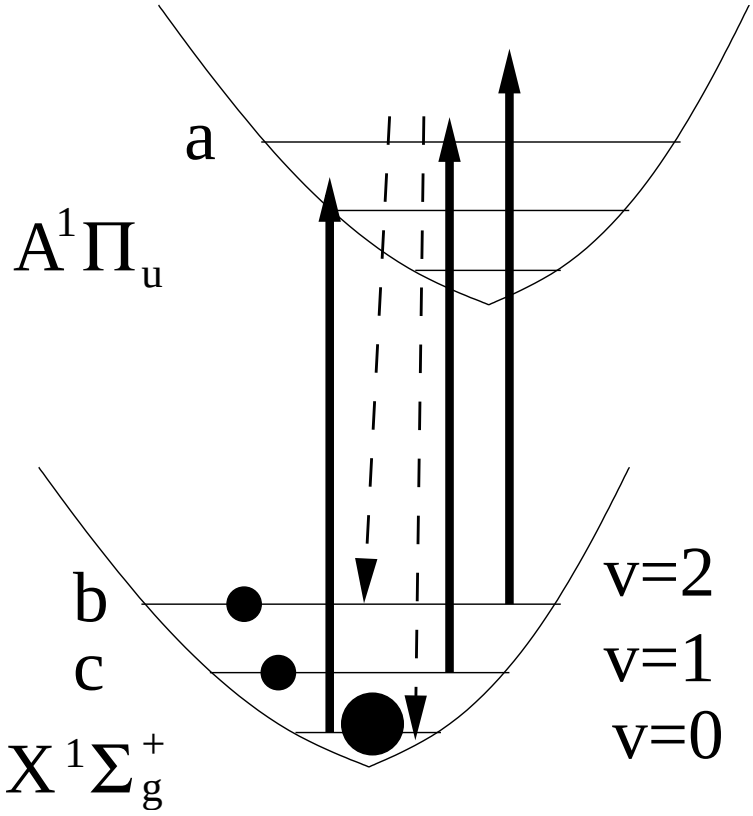

Fig. 17. Molecular level structure of Rb_2.

Vibrational spectral components are very well resolved in scattered spectra presented in Fig. 19. Vibrational energies for ground state are given by

$$\Lambda_v = \omega_e(v + \frac{1}{2}) - \omega_e x_e(v + \frac{1}{2})^2 \tag{2.3}$$

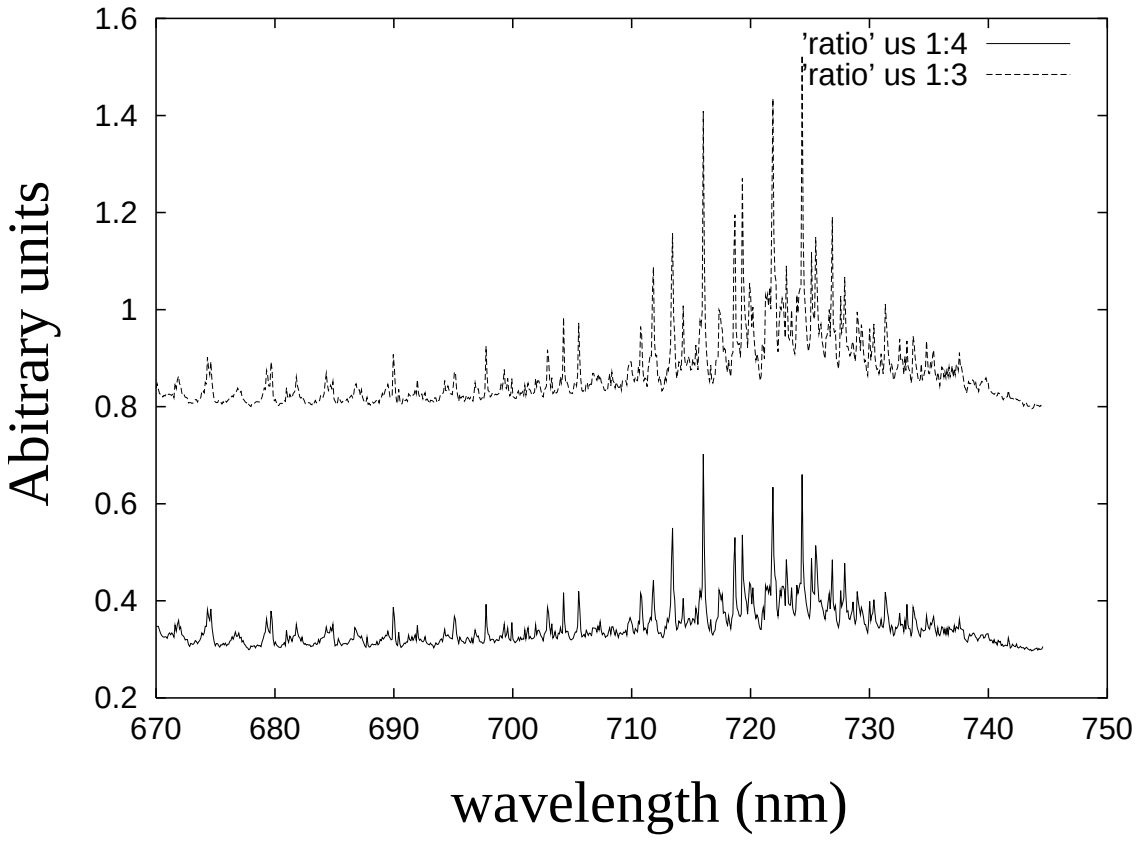

Fig. 18. Scattered Raman spectra

where v is the vibrational quantum number; $\omega_e = 57.58$ cm^{-1} is the vibrational frequency and $\omega_e x_e = 0.15$ cm^{-1} the factor accounting for anharmonizm of the molecular potential energy surface (we used these parameters known from our previous study and literature [33, 15]). We fit the lines by finding vibrational quantum numbers v_1 and v_2 that meet condition $\nu_s = \nu_l + \Lambda_{v_1} - \Lambda_{v_2}$ as seen in Fig. 19.

We have recorded scattered radiation for two cases: first, when the fiber pigtail is in the central part of the scattered emission shown in Fig. 18a, and second, when the fiber pigtail is shifted outside collimated part of scattered light (shift 0.3 cm) shown in Fig. 18b. We take ratio of these two signals and obtain spectral dependence shown

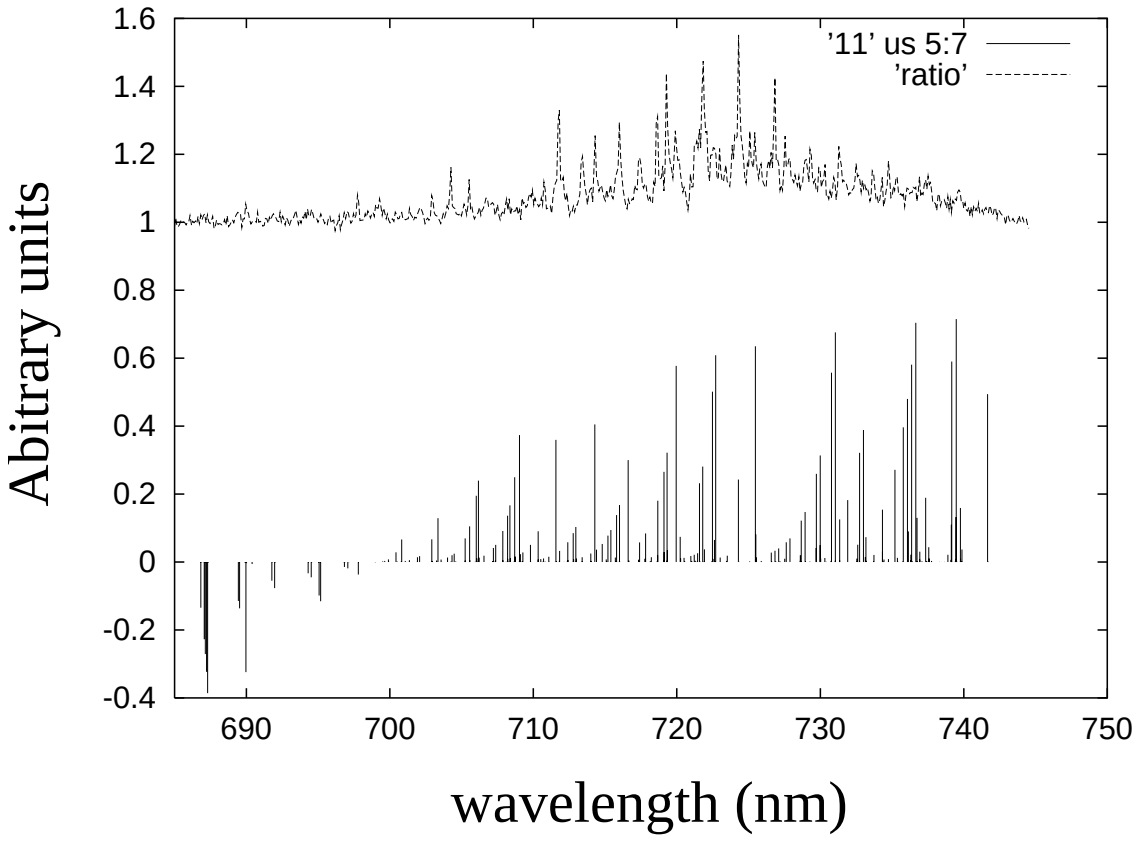

Fig. 19. Raman gain of experiment and theoretical calculation

in Fig. 19a. To obtain the intensity of scatterd light one needs to integrate over the cell taking into account absorption or amplification of the medium which is given

$$I_s(\omega) = \int_0^L dz I_0(\omega) \exp(-\alpha(\omega) z), \tag{2.4}$$

where $I_0(z, \omega)$ is the intensity of the scattered light at frequency ω and position z; $\alpha(\omega)$ is the absorption coefficient, L is the length of the medium where scattering occurs. Neglecting space dependence of scattering intensity $I_0(z, \omega) \simeq I_0(\omega)$, we

obtain by integration

$$I_s(\omega) \simeq I_0(\omega)\frac{1-\exp(-\alpha(\omega)L)}{\alpha(\omega)}. \tag{2.5}$$

One can see that, in dense absorptive media ($\alpha > 0$), scattered light intensity does not depend on the path inside medium L while in the case of $\alpha < 0$ (amplification), there is dependence on L which leads to an angle dependence of the observed intensity of the scattered light. Experimental data shows that, for some lines, the intensity of the scattered light is the same, but for some other lines, the backscattering intensity of the scattered light is higher than the intensity at a small angle. These results we interpret as evidence of Raman amplification.

To support this interpretation, let us analyze the susceptibility of the molecular medium. Even though, the system has many levels, let us first, to gain physical insight, consider just three levels (marked by a, $b(v = 2)$ and $c(v = 1)$ in Fig. 29). For these three levels, the coherence between vibrational levels can be calculated. It is this coherence that makes a major contribution to Raman gain of molecular medium. Thus the effect of the fields in two-photon resonance is taken into account. We neglect the influence of weak fields of fluorescence between electronic levels. The driving field coupled between other ground and excited levels are off two photon resonance, so there is only contribution to power broadening. Thus, the susceptibility given from these three levels is given [1] by

$$\chi(\omega) = i\eta\frac{n_{ab} + \dfrac{\Omega_R^2}{\Gamma_{cb}\Gamma_{ca}}n_{cb}}{\Gamma_{ab} + \dfrac{\Omega_R^2}{\Gamma_{ca}}}, \tag{2.6}$$

where n_{ab} and n_{bc} are the population inversion between levels a and b and between levels b and c correspondingly; Ω_R is the Rabi frequency of the driving field; $\Gamma_{ab} = \gamma_{ab} + i\Delta$; γ_{ab} is the relaxation rate of the molecular coherence; $\Delta = \omega_{ab} - \nu_p$ is the

detuning from the resonance; $\eta = 3\lambda^2 N\gamma_r/8\pi$; the transition frequency ω_{ab} is given by:

$$\omega_{ab} = \omega^e + \omega'_e(v' + \frac{1}{2}) - \omega'_e x'_e(v' + \frac{1}{2})^2 \\ -[\omega''_e(v'' + \frac{1}{2}) - \omega''_e x''_e(v'' + \frac{1}{2})^2] \tag{2.7}$$

where v' and v'' are the vibrational quantum numbers. We take into account thermal population on the vibrational levels $n_v = n_{v=0}\exp[-\Lambda_v/kT]$. Doppler broadening can be taking into account by averaging over the thermal distribution function $F_D(v)$ of velocities v

$$\chi = \int dv F_D(v)\chi(v,\omega). \tag{2.8}$$

Finally we take into account for all the other vibrational levels of diatomic molecule molecule in both the ground and the excited electronic states.

The results of calculation (note that we have not calculated Frank-Condon factors for these lines) are shown in Fig 19. where one can see that it is in qualitative agreement with the experimental ratio of scattered light on and off the axis. To obtain quantitative agreement, we need to measure the field distribution more accurately and take into account Frack-Condon factors.

4. Conclusion

In conclusion, we have observed Raman gain in the backward direction in rubidium diatomic molecules. We have performed simulations that support this interpretation. Note here that what lasing in diatomic molecules via optically pumped population inversion in the excited electronic states has previously been demonstrated in other diatomic molecules (see, for example, optically pumped lasers with Li_2 [35, 36], Na_2 [35, 36, 37], K_2 [35, 38, 39]).

CHAPTER III

QUANTUM COHERENT EFFECTS IN CESIUM DIMER

A. Saturated absorption spectroscopy of cesium molecules

We study sub-Doppler saturation resonances at cesium molecular transitions in the absorption band $B^1\Pi_u \leftarrow X^1\Sigma_g^+$ near 780 nm by using a commercial diode laser. The saturation power is measured as low as 5.7 mW with the laser beam diameter of 0.1 cm. Optical saturation is associated with velocity selective optical pumping of molecular ground state levels. We propose to use the molecular transitions as references for doubled frequency sources in the communication band around 1550 nm.

1. Introduction

Cesium diatomic molecules have a strong absorption band $B^1\Pi_u \leftarrow X^1\Sigma_g^+$ starting at near 750 nm and covering more than 50 nm to the infra-red[40]. The band is densely filled by electric dipole allowed transitions with a typical frequency splitting of the order of the Doppler broadening 0.01 cm^{-1} and can be used as frequency references for stabilization of diode lasers directly or through second harmonic generation (SHG) for frequency stabilization of communication diode lasers in the spectral region 1500 - 1600 nm by applying the SHG technique. Earlier spectroscopic investigations of the absorption band $B^1\Pi_u \leftarrow X^1\Sigma_g^+$ with sub-Doppler resolution were performed with two tunable dye lasers to select coupled transitions.

In this paper we report the observation of sub-Doppler saturation resonances at the cesium molecular transitions with modest pump power (a few mW) from a commercial diode laser. The long relaxation time of ground states and the optical

pumping (depletion) of molecular ground states are demonstrated.

2. Experimental results

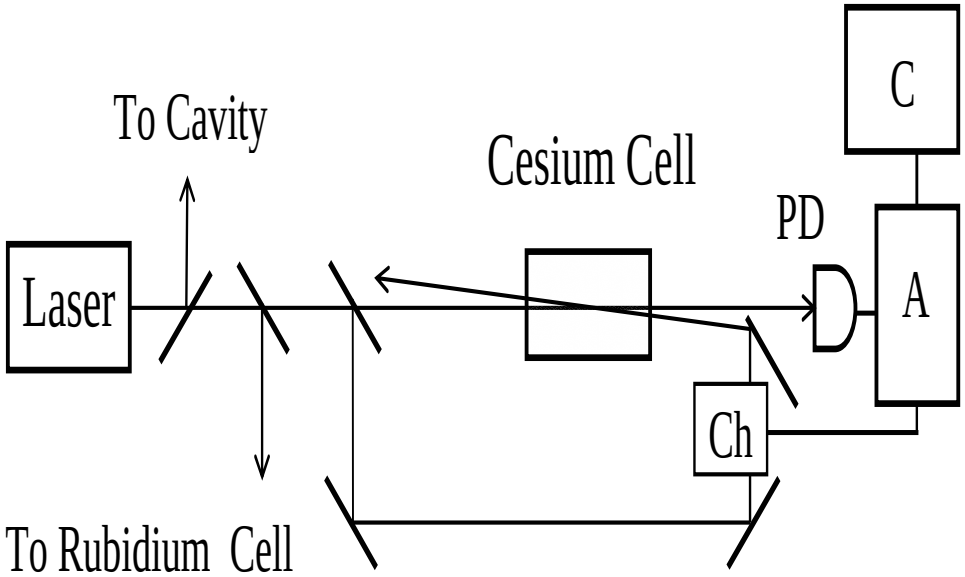

Fig. 20. Experimental setup of saturated absorption in Cs_2: LD - laser diode, Ch - chopper, PD - photodetector, A - lock-in amplifier, C - computer

The experimental scheme is presented in Fig. 20. A free-running laser diode Sanyo DL7140-201S is used in experiment. The line width of the diode laser slowly drifts over interval 10 to12 MHz probably due to a small optical feedback from optical elements before the isolator. The laser frequency can be linear scanned by changing an injection current. The output laser beam is split into several beams. Two laser beams, pump and probe, are sent to a glass cell with cesium vapor in counter-propagating geometry. The probe beam power (0.06 mW) is much less then the pump beam power. The diameters of the pump and probe beams are equal to 0.1cm. The commercial available glass cell (Opthos Instruments, Inc) is installed in an oven. The length of the cell is of 7.5 cm. Vapor pressure of cesium atoms and molecules is controlled via

the temperature of the cell. After the cell the probe beam is sent to a photo-detector. The signal from the photo-detector can be directly analyzed by a digital oscilloscope. Also, in order to select only the non-linear response of the sample, the pump beam is modulated by a chopper. The modulated component of the signal is amplified by a lock-in amplifier and recorded by a computer. We select several molecular transitions between vibrational levels $\mu_e = 5$ and $\mu_g = 10$ in the neighborhood of rubidium atomic transitions at 780 nm. The frequencies of the atomic rubidium transitions are measured with very high accuracy. The Doppler-free absorption spectrum of atomic $^{8}7$Rb vapor serves as the frequency reference. The frequencies of the molecular sub-Doppler resonances are measured relative to absolute frequency of the rubidium transition $5S_{1/2}(F = 2) - 5P_{3/2}(F' = 3)$. The frequency scale is checked by a confocal cavity with a free spectral range of 300 MHz.

The observation of the non-linear response of cesium molecules in the cell is presented in Fig. 21. The curves are recorded at the cell temperature 230^oC. The total atomic and molecular gas pressure is 2.410^{-1} mm Hg (Ntot = $4.610^{15}cm^{-3}$) and the cesium molecular gas pressure is 6.510^{-4} mm Hg (Nmol = $1.310^{13}cm^{-3}$). The curve (a) in Fig. 21 represents the sub-Doppler structure observed with the pump beam power of P = 7.5 mW. The pump and probe beams have a small angle between them 510^{-3} radians, and cross in the central part of the cell. The strongest saturation resonances are marked as R1 - R5. The resonances are near 7% of maximal linear absorption which is 0.15 at frequencies R1 and R2. The contrast of saturation resonances is reduced due to overlap of the Doppler-broadened molecular transitions.

At least two processes can contribute to the saturation of absorption: 1- saturation of an optical transition, 2 - velocity selective optical pumping of ground state levels. If the lifetime of the ground state population distribution is much longer than the lifetime of the excited state population, optical pumping gives the main contri-

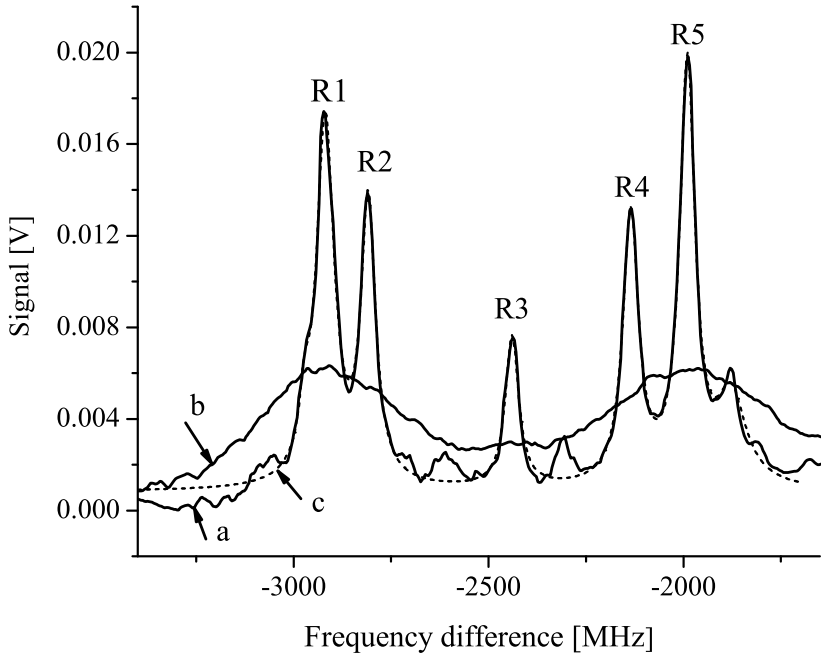

Fig. 21. The saturation resonances at cesium molecular transitions.
curve (a) - sub-Doppler resonances observed with overlapped laser beams;
curve (b) - saturation resonances observed with separated beams;
dotted curve (c) - the fit by Lorentzian functions. Difference frequency is measured relative to the Doppler-free resonance at the atomic rubidium transition $5S_{1/2}(F = 2) - 5P_{3/2}(F' = 3)$

bution to the non-linear variation of molecular absorption. In order to check the contribution of optical pumping, we study the non-linear response of cesium molecules with spatially separated, parallel, pump and probe beams. A similar approach with separated beams was applied for observation of a long lived Larmor precession of Na atoms11, and for observation of a long lived ground state coherence (quantum state memory of light) in Rb atoms. The curve (b) in Fig. 21 presents the non-linear response recorded with a space between beams of 0.3 cm. There is no overlapping of

the beams in the cell. The distribution of optical intensity is checked by a line CCD camera. The spectral shape of the non-linear part of absorption, shown in Fig. 21, reflects the shape of the Doppler-broadened linear absorption lines. It occurs due to velocity changing collisions between cesium molecules and cesium atoms. One can see that there is practically no Doppler-broadened background in the curve (a). It means that the free mean path for velocity changing collisions is more than the beam diameter 0.1 cm and less than the beam separation 0.3 cm. Therefore in the case of overlapped beams (Fig. 21, the relaxation time of the ground state population is defined by time-of-flight of the molecules through laser beam, and can be roughly estimated to be 10^{-5} sec. The optical saturation is associated with selective optical pumping of the molecular ground state levels. Collisions with cesium atoms do not destroy the ground state population distribution in the cesium molecules, they change only the velocity distribution of the cesium molecules. In the mixture of cesium atoms and cesium molecules the atomic vapor is working as a buffer gas, for instance, like neon atoms for sodium atoms. Resonance exchange effects between cesium atoms and molecules are small due to a big energy difference between resonance atomic and molecular transitions (wavelengths of cesium D2 and D1 lines are 852 nm and 895 nm).

The sub-Doppler resonances are fit by Lorentzian functions. The fit is shown in Fig. 21 as a dotted curve (c). Full-width at half maximum $\Delta\omega$of the strongest five resonances varies from 42 to 55 MHz. We measure the power broadening of the narrowest and the most isolated resonance R3. The results are presented in Fig 22. From the fitting by the well known expression for power broadening10,15 $\Delta\omega = \Delta\omega_0[1+(1+P/P_0)^{1/2}]/2$, we have obtained the magnitudes of saturation power, P0 = 5.7 mW, and the low power limit of the width $\Delta\omega_0 = 32MHz$. By taken into account the laser line width and the residual Doppler broadening we have estimated

the minimal width of the selected saturation resonance as 20 MHz. The saturation intensity can be written as $I_0 = P_0/S \sim [\Delta\omega_0/(Td_{ge}^2)]$, where d_{ge} is effective dipole moment of the optical transition, T is the effective lifetime of population difference between ground and excited state, and S is the laser beam area. When the condition for ground state optical pumping is satisfied (the ground state non-equilibrium population lifetime is much longer than the excited state lifetime) the saturation effects are enhanced. The ground state optical pumping in cesium molecules helps to compensate the relatively small electric dipoles of the molecules.

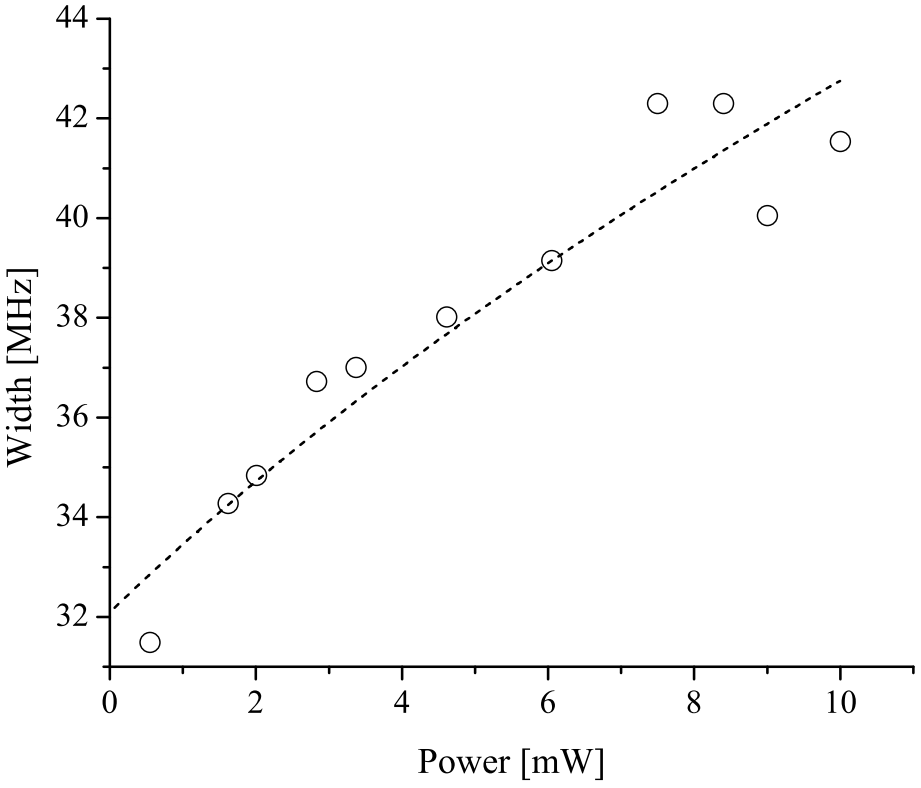

Fig. 22. Power broadening of the saturation resonance R3 in Fig. 21. The experimental data (circles) and the fit are presented

The spectral shapes of the sub-Doppler resonances are studied at different temperatures from 195 C to 260 C. The vapor pressure induced variation of the resonance width and shift is less then 2 MHz in this temperature region. The spectral resolution is limited by the drift of the laser line width. Populations of molecular ground state sub-levels are not destroyed by molecular-atom collisions.

3. Conclusion

The cesium molecular absorption lines in the band B1u X1g+ can be considered as frequency references. The sub-Doppler absorption resonances in the another cesium band $A^1\Pi_u \leftarrow X^1\Sigma_g^+$ were used for frequency stabilization of diode lasers (1083 nm)16 and Nd:YAG lasers (1064 nm). The Nd:YAG laser frequency stability was reached a minimum 1.310^{-11} for a measurement time of 20 s. These results support our proposal to use the absorption lines in the shorter wavelength band $B^1\Pi_u \leftarrow X^1\Sigma_g^+$for frequency stabilization of frequency-doubled communication lasers in the spectral window around 1550 nm. Also the observation of ground state optical pumping in cesium molecular vapor shows that it is possible to observe electromagnetically induced transparency (EIT) in a -levels scheme in diatomic molecules. Recently EIT was observed in cascade systems in Li^2 and K^2 molecules. It opens the way to realize the quantum state memory of light in a molecular gas.

B. Λ scheme electromagnetically induced transparency

1. Introduction

Coherent effects such as electromagnetically induced transparency (EIT) and coherent population trapping (CPT) [7, 41] attract a lot of attention because of their ability to suppress a linear absorption and enhance the non-linear response of a resonant medium. These complimentary coherent effects impact new techniques such as high precision spectroscopy [42, 43], atomic clocks [44], nonlinear interaction with weak light fields at the single photon level [45, 46, 47], greatly reduced phase matching requirements [48], large Kerr nonlinearities [49], etc.

The CPT was first reported in [50], where the elimination of resonant fluorescence of sodium atoms was observed under conditions where the mode spacing of a multi-mode dye laser was equal to the ground state splitting. Description of other experiments with CW lasers can be found in the review. The CPT has also been observed in the pulsed regime [51]. CPT in sodium dimers has been observed in [52, 53].

Growing interest in EIT was stimulated by Harris's theoretical work [54]. EIT has been successfully demonstrated in different experiments: in continuous wave and pulsed regimes [54]; with atomic gases at room temperature [55, 56] or with cold atoms [57], with solids doped by rare-earth ionsand semiconductor quantum wells ; for different wavelengths ranging from gamma-rays, optics to microwaves [55, 54, 58, 59].

In this paper, we have experimentally demonstrated EIT in Cs dimers vapor within the transition band $B^1\Pi_u \rightarrow X^1\Sigma_g^+$ and performed simulations to support our experimental results.

The structure of the paper is the following. In the next section we describe the experimental setup has been used. Then, we discuss the obtained results and present

simulations that supports the observed results.

2. Experimental setup

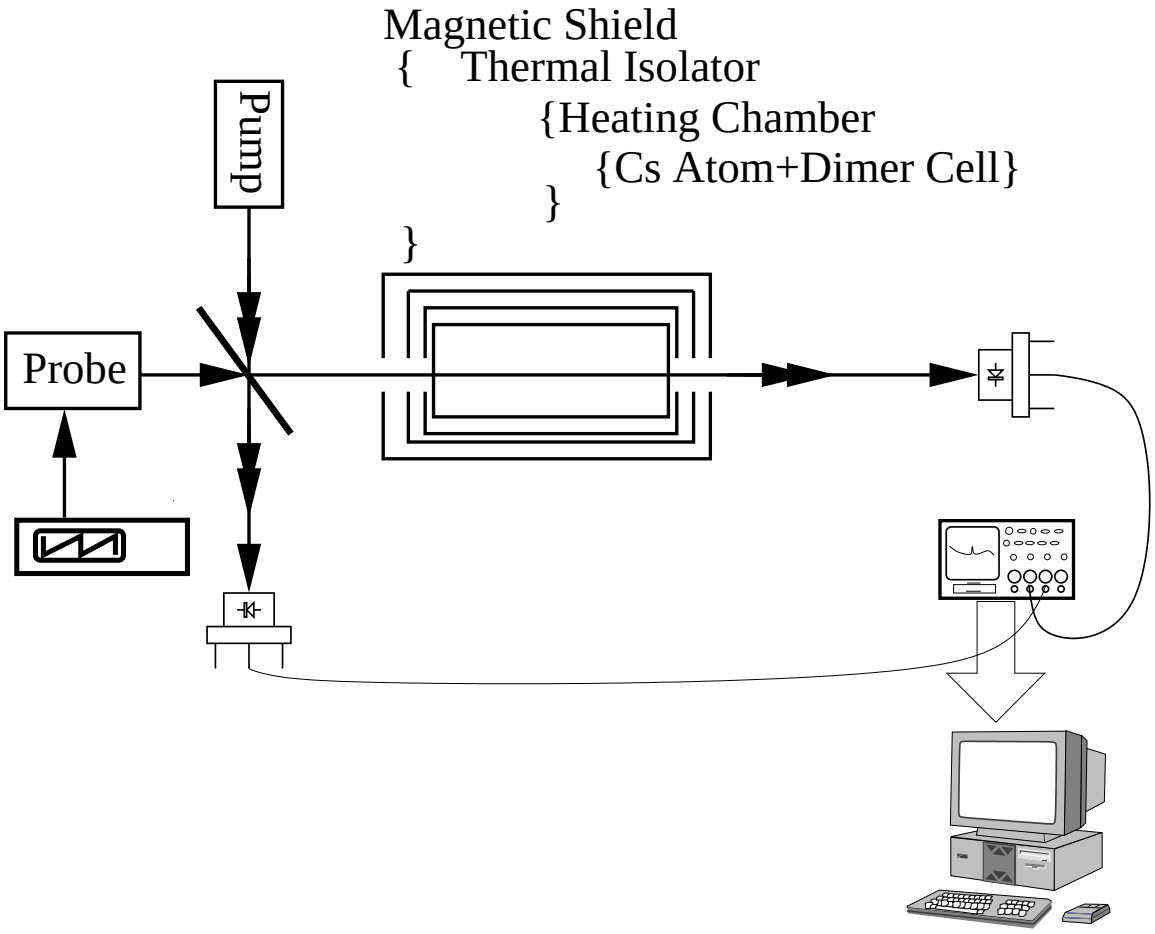

Fig. 23. Experimental setup of electromagnetically induced transparency in diatomic cesium molecular gas

The experimental setup is shown in Fig. 23. The outputs of two external cavity diode lasers operating around 780nm are used to pump Cesium diatomic molecules from ground electronic state to $B^1\Pi_u$ state and to probe at very close frequency to form the Λ type electromagnetically induced transparency. The third free running laser is used to beat these two lasers on detectors, the beating signals are used to

compare with signal from a Rubidium absorption lines to get accurate frequency of pumping and probing laser.

The Cesium metal sample, is placed in a cylindrical pyrex glass cell (75mm long and 25 mm in diameter). A thermocouple is placed in touch with the cold spot of the cell to monitor the temperature of Cesium vapor. The cell is placed inside an oven and heated to above 500 Kelvin. The cell and oven are inside a magnetic fild shield to minimize any effect from earth magnetic field. For the temperature from 470K to 520K, the density of Cesium dimer is from 10^{13} to 10^{14} cm^{-3}. the atomic Cesium density is from 10^{15} to 10^{16} cm^{-3}.

To characterize spectral resolution of the experimental setup, we measure the beat note signal between pump and probe lasers, the beat note signal was sent to spectrum analyzer, it is shown in Fig. 24, we can see that the width of the two laser measured ia as narrow as 0.5 to 0.7 MHz.

3. Obtained results and discussion

Cs dimers have several absorption band, the one from 750nm to 800nm correspondent $B^1\Pi_u \leftarrow X^1\Sigma_g^+$. With pumping at ω_0 and probing at ω_1, we get very narrow peak width as 2Mhz, it is narrower than the nature line width.

Cs_2 dimer molecule in the ground state ($X^1\Sigma_g^+$) absorbs a photon to get excited to the electronic state $B^1\Pi_u^+$ see schematic level structure of Cs_2 shown in Fig. 29. Because the vibrational energy for Cs_2 is much smaller than kT, the population is distributed by thermal motion among vibrational levels of the ground state, and hence there are many absorption lines originated from the ground state.

Vibrational spectral components are very well resolved in scattered spectra pre-

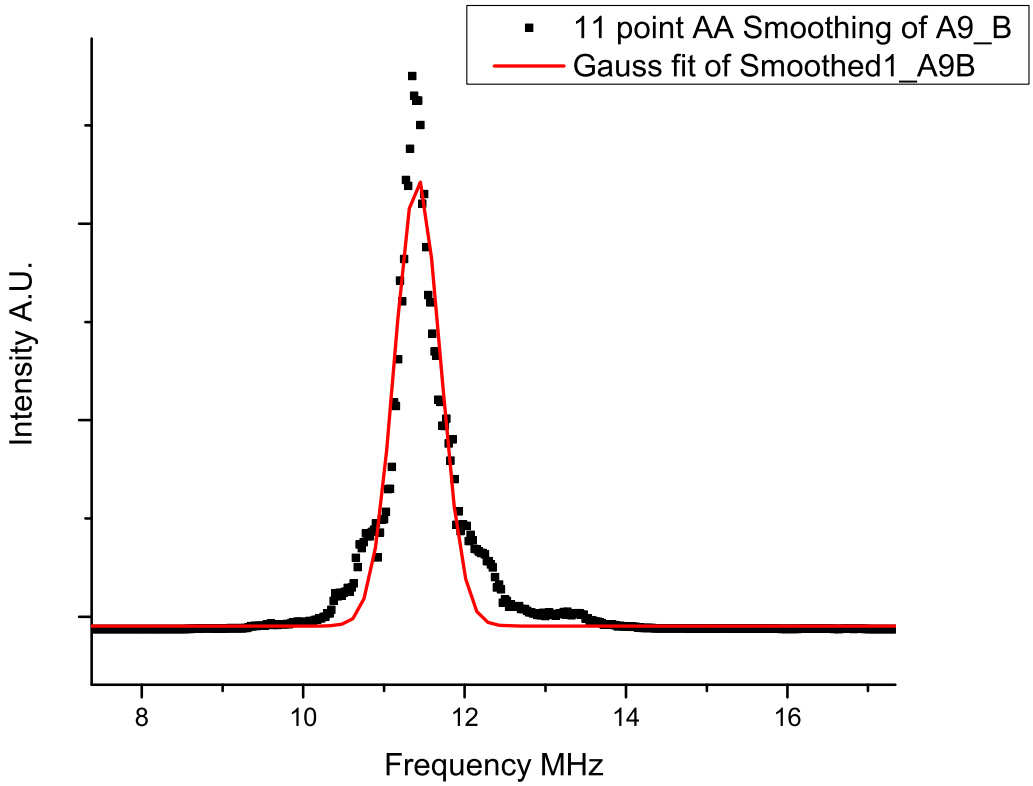

Fig. 24. Probe and drive laser beat signal width

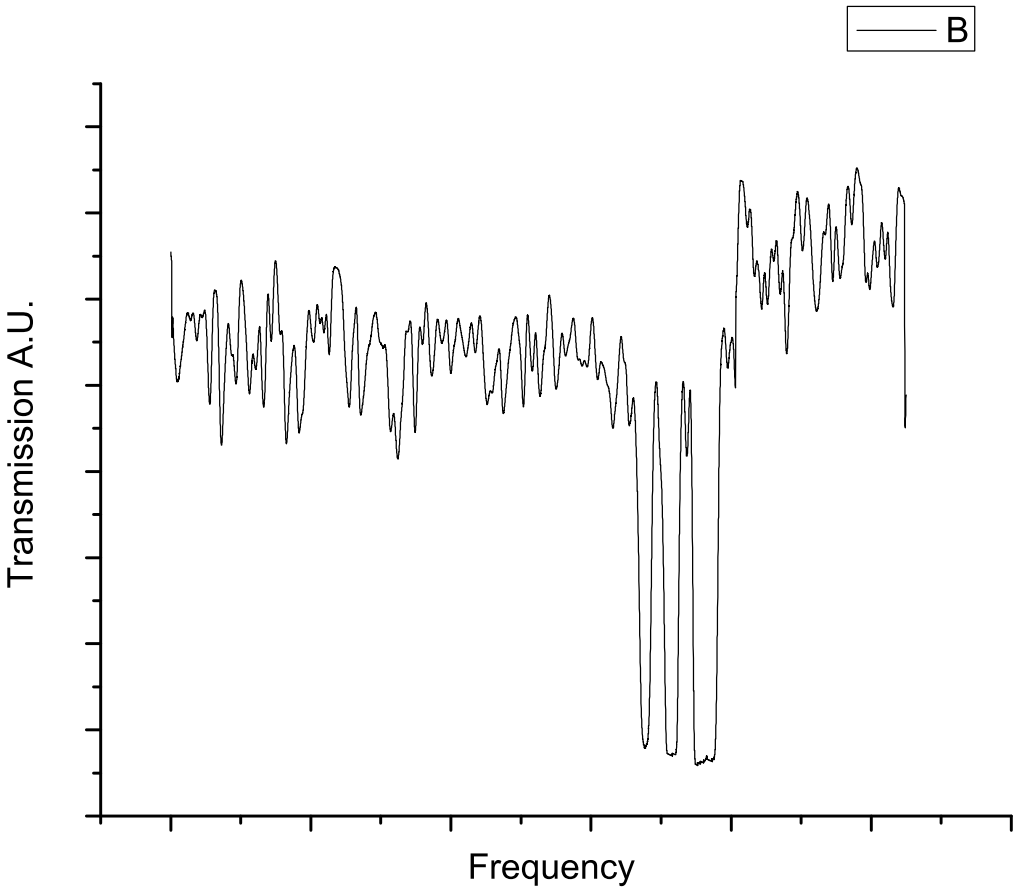

Fig. 25. Cs2 broadband absorption

sented in Fig. 25. Vibrational energies for ground state are given by

$$\Lambda_v = \omega_e(v + \frac{1}{2}) - \omega_e x_e(v + \frac{1}{2})^2 \tag{3.1}$$

where v is the vibrational quantum number; $\omega_e = 57.58$ cm^{-1} is the vibrational frequency and $\omega_e x_e = 0.15$ cm^{-1} the factor accounting for anharmonizm of the molecular potential energy surface.

In the current experiments, we drive the Cs_2 molecular system with a relatively

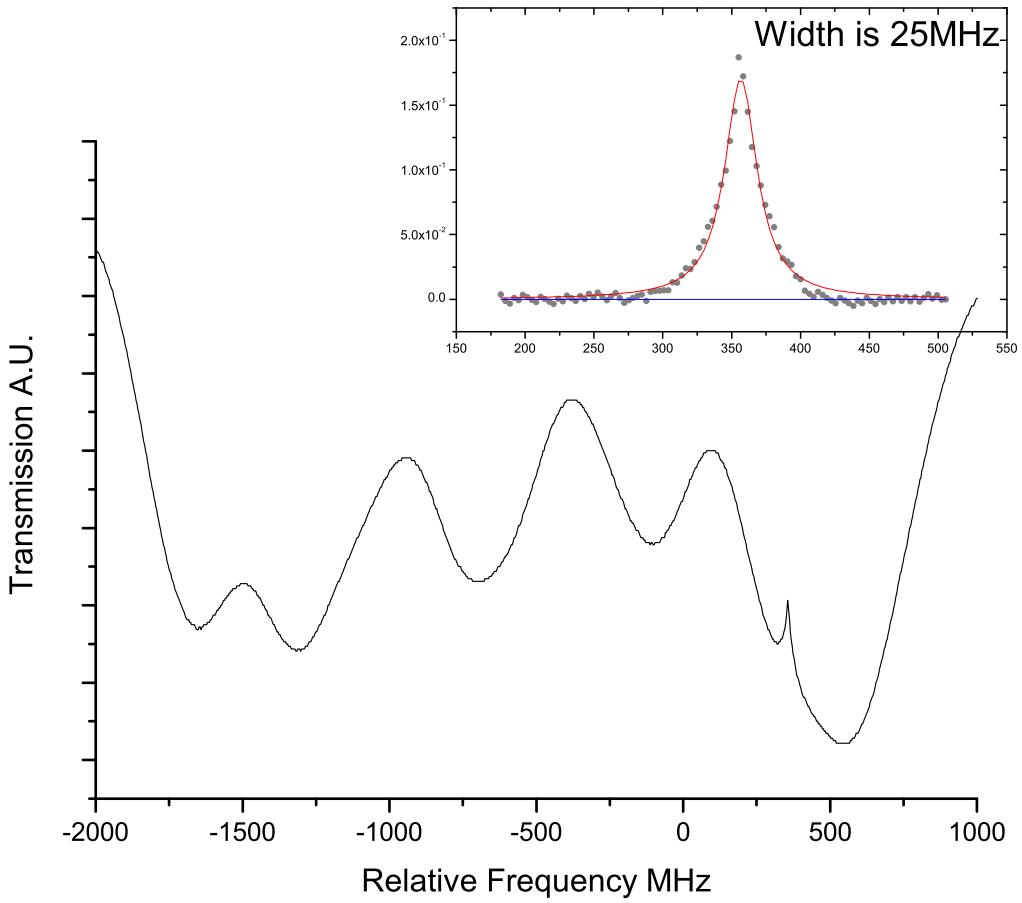

Fig. 26. Cs2 EIT experiment: pump laser Doppler free peak width and frequency

strong CW laser field and simultaneously we measure transmission of a relatively weak probe laser.

First, we measure the width of by using Doppler free saturation spectroscopy for the this we fix the frequency of the drive laser and scan the frequency of the probe laser around the frequency of the drive laser. The obtained results are shown in Fig 26. The beat signal of two lasers shows the peak width that is corresponding to the co-propagating doppler free, the width is about 25MHz.

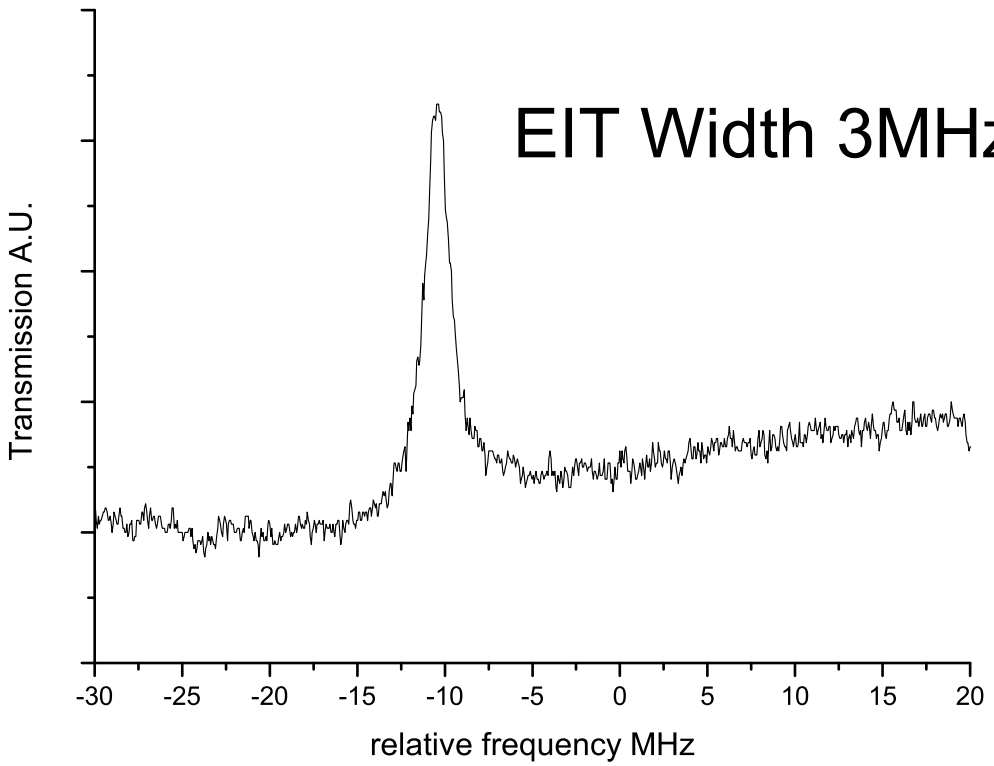

Fig. 27. Cs2 EIT narrow peak in the transmission spectra of probe laser

Next we turn to study transparency for larger detuning of the probe laser. When the probe frequency is in two-photon resonance with the drive, we observe enhancement of transparency in a narrower region, as shown in Fig 28. Since at the same pump laser frequency, we also have observed a sub-natural EIT width.

The examples of different EIT widths are shown in Figs. 28 and 30. These plots are obtained for different densities of Cs dimers. By changing the temperature of the cell, we have also study the dependence of EIT width on the Cs dimer density. The narrowest width is about 3 MHz.

Also it turns out that we manage to find V-type scheme configuration. This EIT

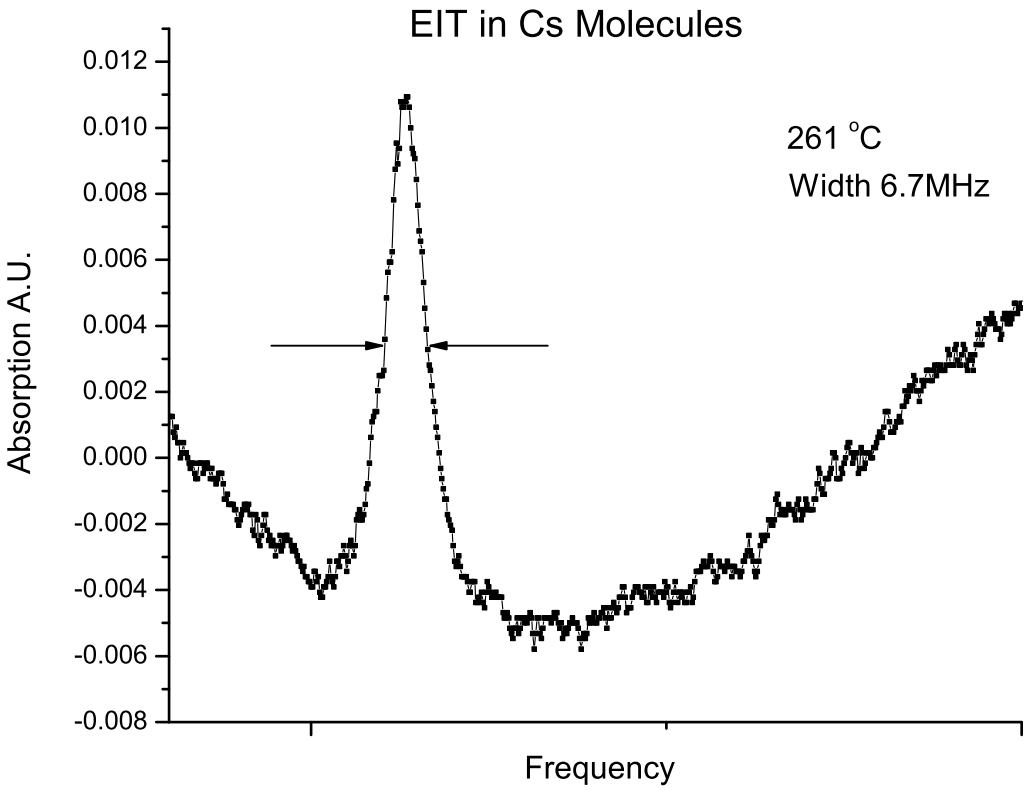

Fig. 28. EIT peak at high temperature

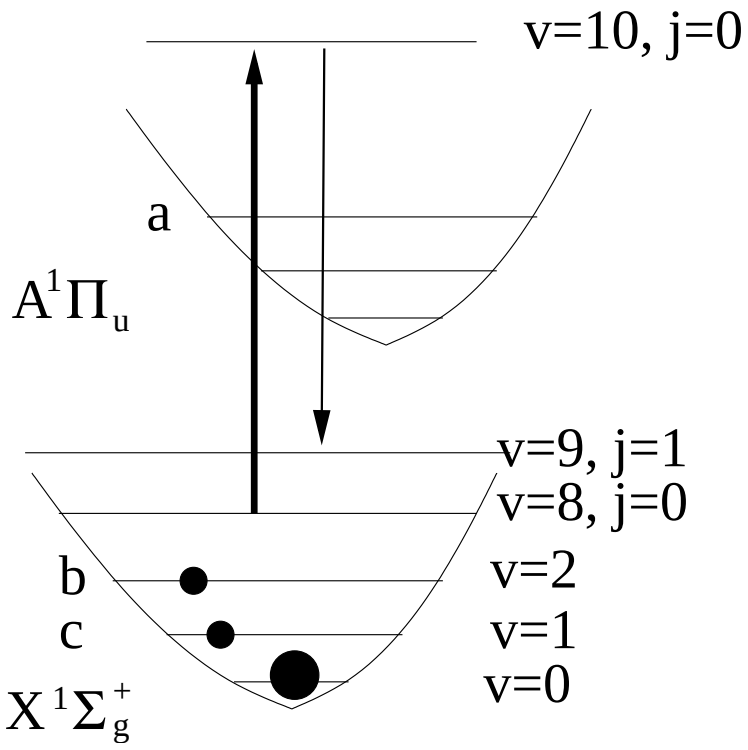

Fig. 29. Molecular level structure of Cs_2

transparency peak with width is about 40 MHz (as shown in Fig. 31). It is broader than the width of EIT in Lambda configuration because the relaxation of coherence is faster.

4. Λ scheme EIT

The linear transmission signal of the Cesium diatomic molecule is shown in Fig 25. The pump and probe laser frequencies are label on the curve. The two photon detuning is around 62 GHz.

Since we observed both wide and narrow peaks at different probe frequency and the narrow one is narrower than natural line width. Based on the pump and probe analysis, we can tell that we find Λ transition in molecule. while Cascade type EIT was reported in some's paper.

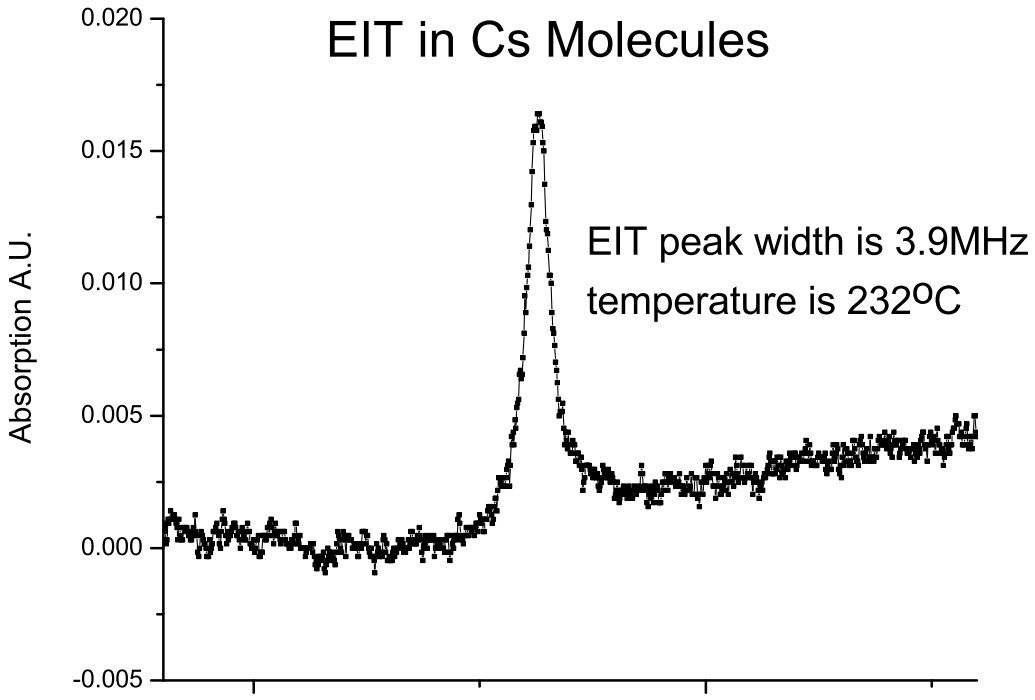

Fig. 30. EIT peak at lower temperature

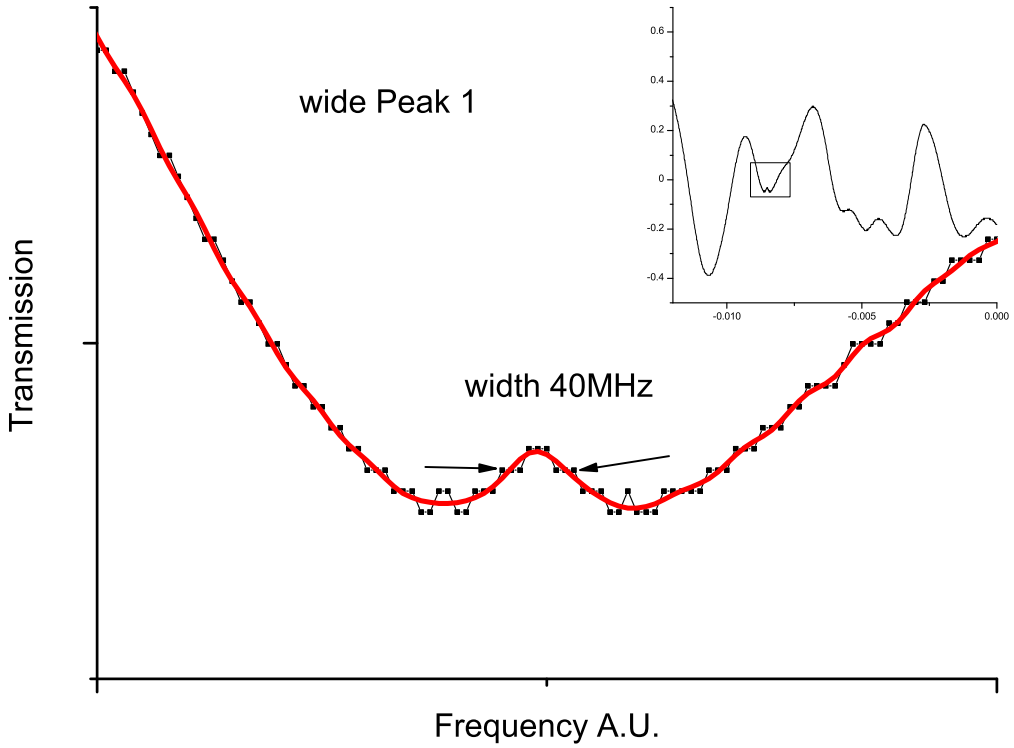

Fig. 31. Transmission peak of V type EIT

Based on the Dunham Coefficients of $X^1\Sigma_g^+$ and $B^1\Pi_u$ from Demtröder's and Amiot's papers. we calculated the transition energy and Franck Condon factor of the transition it shows that the electronic transition is B-X,vibrational is 6-11 and rotational 88-90.

We fit EIT peak width with temperature with exponential function. It gives an acceptable result showing that the EIT peak width has exponential dependency on temperature.

In Fig 32, we present the dependence of the EIT peak width on the temperature. We fit the curve with an exponential increasing function, we get the extrapolate EIT peak width at zero temperature is around 1.7 MHz. in the real experiment we can never decrease our temperature very low since below 170 degree, the linear absorption of cesium dimer becomes negligible.

To make an comparison, Doppler free peak width is also measured over 200 to 260 degree range. In this range there is no obvious density or temperature dependency.

In fig 33, we can see at the working temperature range, there is practically no temperature dependence of Doppler free peak width with temperature. When the temperature is below 210 degree, the width becomes bigger, since at this temperature the density of cesium dimer become so dilute that even same laser power as other temperature measurement will saturate the dimers.

We can calculate rotational quantum number from two photon detuning. since the ground states are in the same electronic states and vibrational state. Then, from the selection rule and energy formula and constants from spectroscopic study of the Cesium dimer, we get the rotational quantum number as 89 and 90 of the ground states and upper state has rotational quantum number 90. We can thereafter determine the vibrational quantum numbers. They are 11 for the ground states and 6 for excited states.

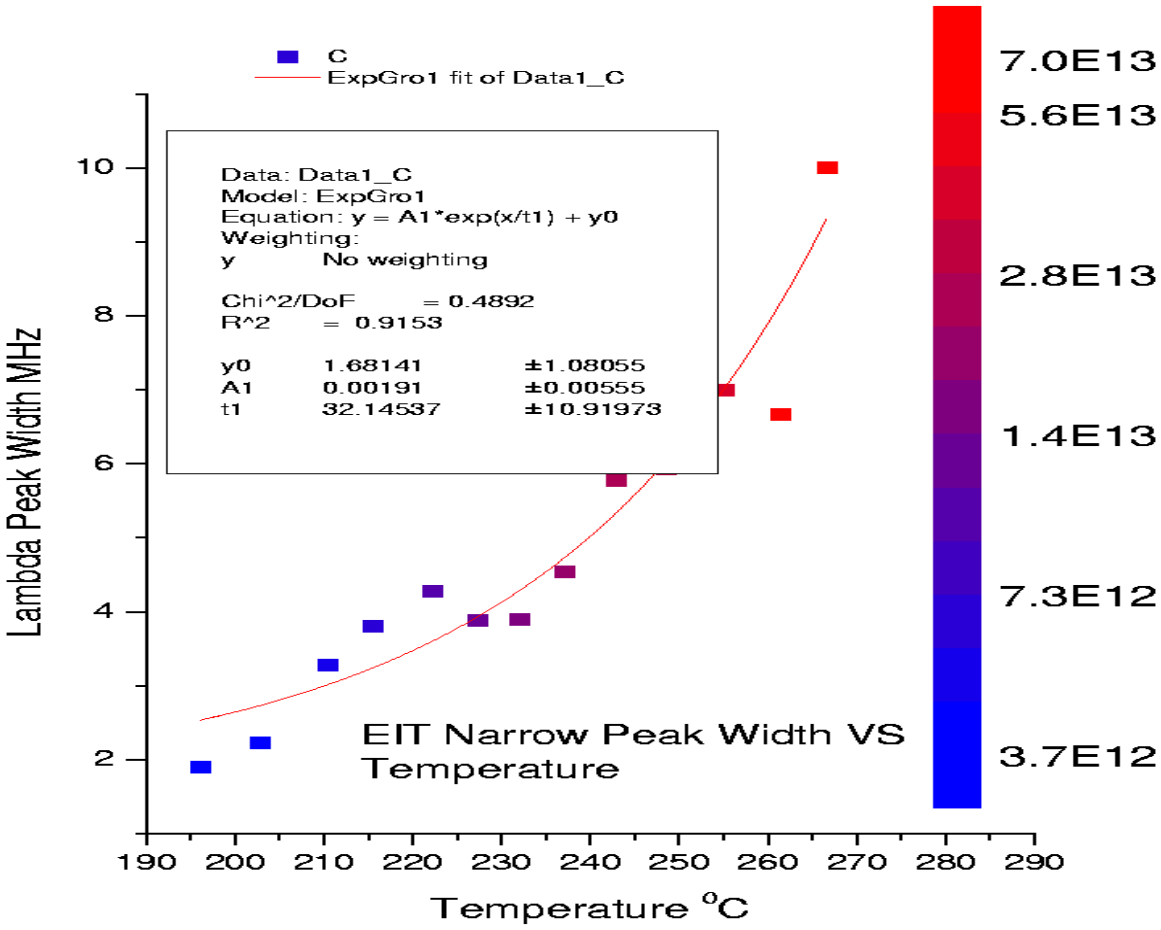

Fig. 32. Width of EIT peak vs. temperature

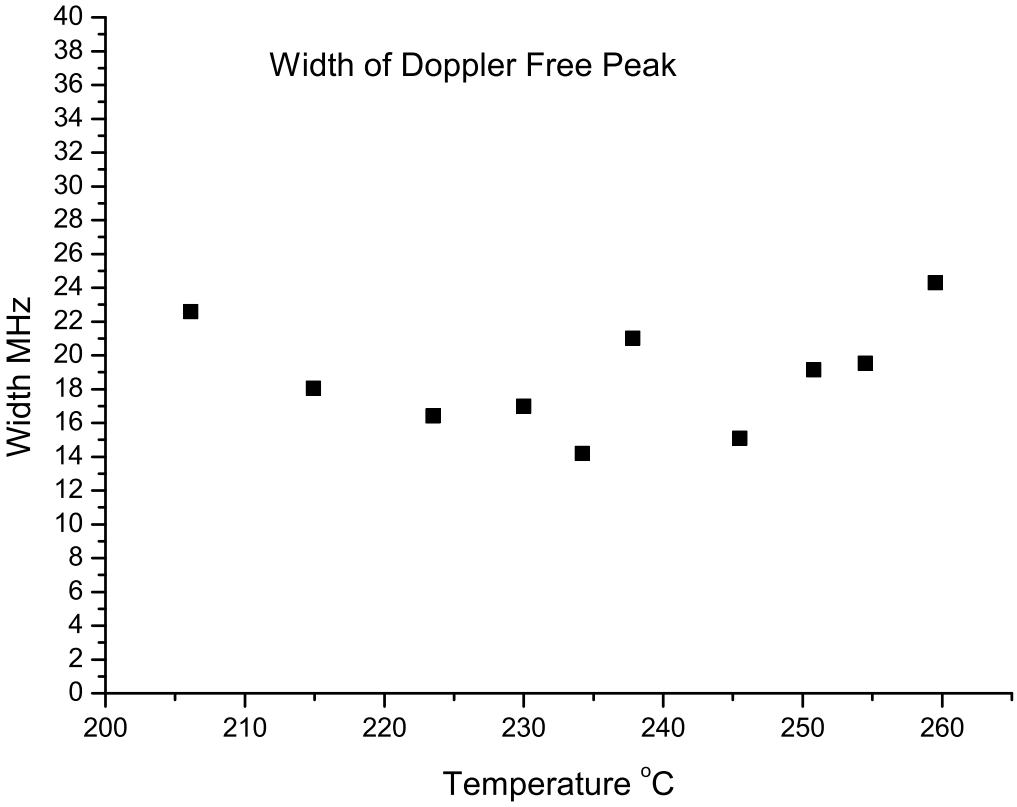

Fig. 33. Width of Doppler free peak vs. temperature

To support the observed results, let us analyze the susceptibility of the molecular medium. Even though, the system has many levels, let us first, to gain physical insight, consider just three levels (marked by a, $b(v=2)$ and $c(v=1)$ in Fig. 29). For these three levels, the coherence between vibrational levels can be calculated. It is this coherence that makes a major contribution to Raman gain of molecular medium. Thus the effect of the fields in two-photon resonance is taken into account. We neglect the influence of weak fields of fluorescence between electronic levels. The driving field coupled between other ground and excited levels are off two photon resonance, so there is only contribution to power broadening. Thus, the susceptibility given from these three levels is given [1] by

$$\chi(\omega) = i\eta \frac{n_{ab} + \dfrac{\Omega_R^2}{\Gamma_{cb}\Gamma_{ca}} n_{cb}}{\Gamma_{ab} + \dfrac{\Omega_R^2}{\Gamma_{ca}}}, \tag{3.2}$$

where n_{ab} and n_{bc} are the population inversion between levels a and b and between levels b and c correspondingly; Ω_R is the Rabi frequency of the driving field; $\Gamma_{ab} = \gamma_{ab} + i\Delta$; γ_{ab} is the relaxation rate of the molecular coherence; $\Delta = \omega_{ab} - \nu_p$ is the detuning from the resonance; $\eta = 3\lambda^2 N\gamma_r/8\pi$; the transition frequency ω_{ab} is given by:

$$\begin{aligned} \omega_{ab} = \omega^e + \omega'_e(v' + \frac{1}{2}) - \omega'_e x'_e(v' + \frac{1}{2})^2 \\ -[\omega''_e(v'' + \frac{1}{2}) - \omega''_e x''_e(v'' + \frac{1}{2})^2] \end{aligned} \tag{3.3}$$

where v' and v'' are the vibrational quantum numbers. We take into account thermal population on the vibrational levels $n_v = n_{v=0}\exp[-\Lambda_v/kT]$. Doppler broadening can be taken into account by averaging over the thermal distribution function $F_D(v)$ of

velocities v

$$\chi = \int dv F_D(v)\chi(v,\omega). \tag{3.4}$$

Finally we take into account for all the other vibrational levels of dimer molecule in both the ground and the excited electronic states.

5. Conclusion

In conclusion, we have experimentally observed electromagnetically induced transparency in cesium molecular gaseous medium.

With the same drive laser frequency, we observed two kinds of transmission increasing peak, the narrower one is due to Λ type transition, and the broader one is due to V type transition.

The narrow EIT peak width is much smaller than the natural linewidth of the linear transition(single photon transition), which also confirms that the two lower states of Λ type transition belong to the ground states.

The extrapolated curve of the width intersect with y axis at 1.7MHz, subtracting the two laser width 0.7 MHz, there is still 1 MHz left. Time of flight is around $6 \times 10{-}6s$, it gives width of 0.17MHz. The additional width is probably due to rotational relaxation of ground states.

We have performed simulations that support this interpretation.

C. Light storage in a dense diatomic medium

We know that electromagnetically induced transparency can modify the absorption properties of the medium. The basic manifestation of EIT is a significant reduction of light absorption in the medium near a resonance transition frequency.

Using Λ type atoms or molecules, we can realize the light storage. Strong "writ-

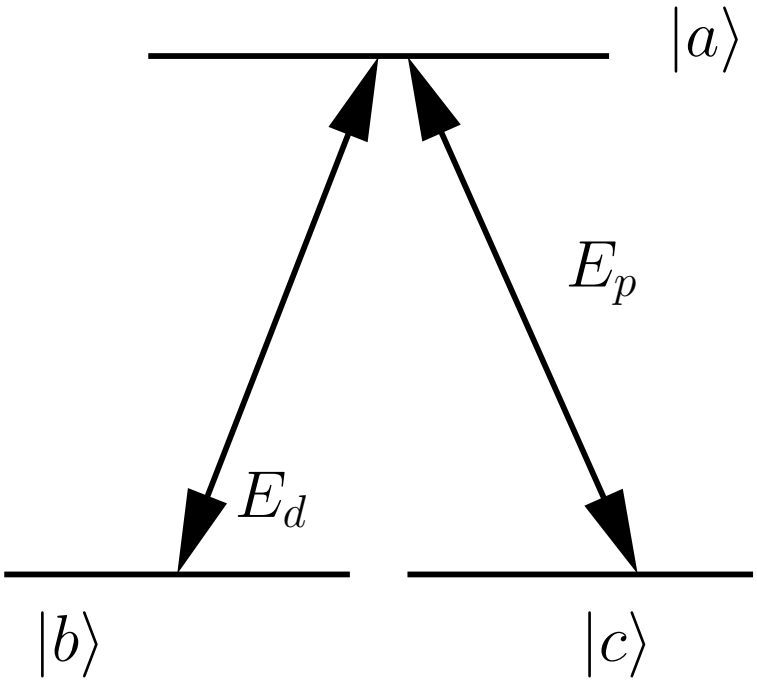

Fig. 34. Configuration of fields in molecular medium light storage. Drive and probe field couple three level atom

ing" and weak "signal" light pulses propagate in a Λ type three level gaseous system and excite a spatial distributed long lived coherence between ground states $|b\rangle$ and $|c\rangle$. This coherence profile stores information about the single probe pulse, once we turn off drive field. Subsequently we send a strong "reading" pulse into the medium, the reading pulse will results Raman scattering off the atomic coherence and generate a "retrieved" pulse. The retrieved pulse can be identical to the signal pulse in the frequency and quantum statistics and propagating direction.

1. Experimental setup

Laser light from a diode laser is split by the beam splitter and then modulated by two acoustic optical modulators. We focus the beam into the AOM to get sharp rising

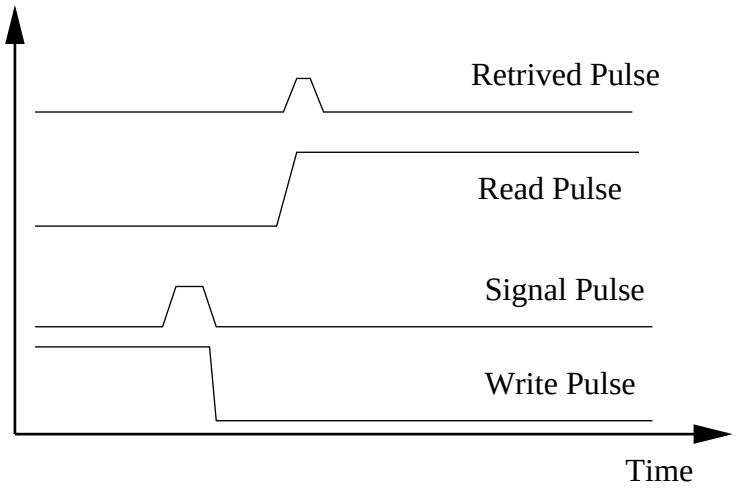

Fig. 35. Illustration of pulses sequences of light storage experiment

edge. One beam is rotated by a half waveplate and then combined with the other beam at the polarized beam splitter. Combined beam go through a quart waveplate to get clockwise and counter clockwise circular polarized light. The beams then go through a Cesium Cell heated to over 200 degree. The beams after the oven then go through a quart wave plate and split by a polarized beam splitter and detected by two fast photodiode.

2. Result of light storage in molecule experiment

The rising and falling edge of light pulse is less than 10 nanosecond. The signal pulse is around 30 nanosecond wide. Both writing and reading pulse are from drive beam. The delay between the falling edge of writing pulse and the rising edge of reading pulse is variable. We can can see the retrieved pulse for delay from 30 nanosecond to around 80 nanosecond. When the delay is bigger than 80 nanosecond the retrieved pulse becomes too small to be observed.

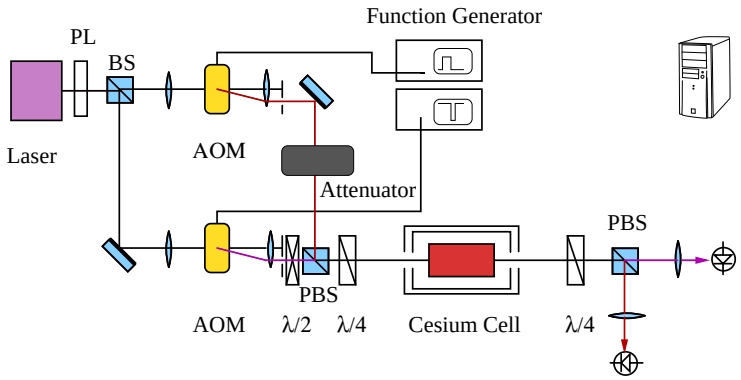

Fig. 36. Light storage experiment setup. Linear polarized light from diode laser is split into two beams and modulated by Acoustic Optical Modulator into pulses, one beam is then converted into perpendicular polarized by a half wave plate. Two beams are combined into one by Polarized beam splitter and converted into circular polarized light by quarter wave plate. The transmission light is detected by two fast photo-detectors

3. Conclusion

From the experiment of electromagnetically induced transparency, we found the EIT width is less than 2 MHz. The corresponding lifetime of ground state coherence is big than 80 nanosecond. In the allowed time region, We have observed the retrieved pulse in the same direction and with the same polarization of the signal pulse.

For diatomic molecule as Cesium dimer, at our working temperature, the most populated rotational quantum number is around 120. We work with circular polarized light of same frequency, therefore we work on the rotational sublevels of Cesium molecule.

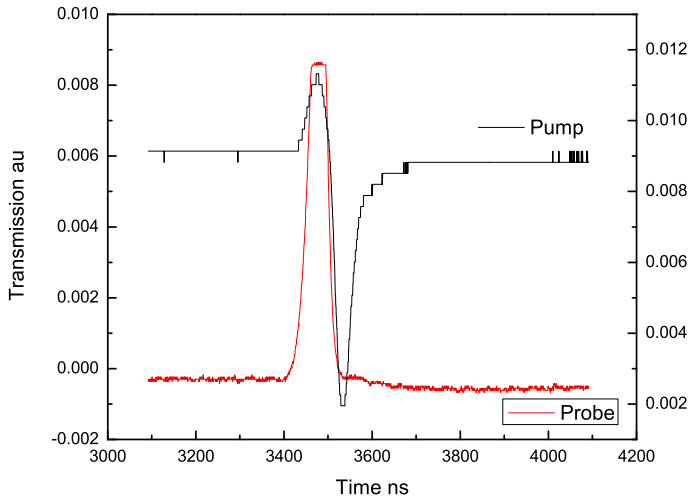

Fig. 37. Light storage result

CHAPTER IV

CHIRAL EFFECT IN RUBIDIUM ATOMS

A. Optically induced chirality in Rb vapor

Atoms and molecules in electromagnetic fields can be considered a new state of matter that continues to attract a great deal of attention. Electromagnetic fields provide a method to manipulate the properties of matter such as absorption, dispersion and a varieties of nonlinear characteristics [60, 61, 62, 63]. Similar to the fabrication of new materials, like photonic crystals or nanostructures, an applied coherent field allows one to improve the performance of devices and go beyond the limitations set by natural materials by themselves. In particular, it creates conditions for lasers to operate without population inversion between levels relevant for the lasing transition. Giant nonlinearities [61] and large refractive indexes [63] have been achieved. Giant nonlinearities may enable one to generate nonlinear signals using single photons [64]. The enhanced nonlinearity can also bring the light pulse to slow down considerably [65, 66, 67] and this is used for quantum information storage [68, 69].

Here we would like to answer the question of whether it is possible to use the quantum coherent effects to enhance the effect of optical activity [70]. Optically active molecules are abundant in nature. In fact, the nearly exclusive utilization of one form of the optical antipode pair may be considered as a characteristic feature of living systems. Optical activity has always stimulated researchers' imagination, as the substitution and modification of natural products is not only a challenge but also of high practical importance. It is important to control chirality or to create an environment that displays chirality in a controllable way, which can have applications in drug production, spin chemistry, etc. In this letter we report the experimental

observation of very large optically induced chirality in a Rb cell.

The chirality of a molecule is a symmetry property: chiral molecules are either asymmetric, i.e. they do not have any symmetry element, or they are asymmetric, i.e. they have only axes of rotation. If an atomic or molecular system has spherical symmetry then the transmission coefficient is the same for light propagating parallel to the magnetic field and for light propagating in the anti-parallel direction with respect to the magnetic field. If a symmetry operation of reflection is performed on a chiral molecule it is transformed into a different chiral system of equal energy and other nonvectorial properties. This molecule is called a mirror image, the optical antipode, or the enantiomer. Molecular systems that show chirality have an obvious or hidden screw property, or a handedness. In the case when the molecule has no symmetry then there is the phenomenon of optical chirality. Arago's discovery in 1811 of natural optical activity in chiral crystals and Faraday's discovery in 1846 of magnetically induced optical activity have contributed much to our understanding of the wave nature of light and the electronic properties of molecules. Both effects are manifest as a rotation in the polarization of transmitted light: the former is due to the intrinsic properties of media that lack mirror symmetry, whereas the latter (which occurs in all materials) is due to magnetic-field-induced changes in the optical properties.

Recently, a new polarization-independent optical effect was discovered: magnetochiral anisotropy (MCA). The existence of this effect may be important in the context of fundamental interactions between light and matter, and in molecular spectroscopy, although the effect is generally very weak for naturally occurring systems [71, 72, 73, 74, 10, 75, 76]. In a recent paper Agarwal and Dasgupta [11] discovered that it is possible to produce very large MCA using electric dipole transitions and by applying a properly polarized coherent field so as to break the symmetry

of the system. We will refer to this type of MCA as electromagnetically induced magnetochiral anisotropy (EIMCA). We note that very interesting experiments on birefringence induced by laser fields in the absence of any magnetic field have been reported [77].

The idea of optically induced chirality is the following. First, consider a simplified model of the Rb atom, a three-level atom (see Fig. 39b); the Hamiltonian of the atom in magnetic and optical fields is given by

$$H = \hbar\omega_+|-\rangle\langle -|\hbar\omega_-|+\rangle\langle +| + \hbar\Omega|+\rangle\langle f| + h.a. \tag{4.1}$$

where $|-\rangle \equiv |m=-1\rangle$, $|+\rangle \equiv |m=+1\rangle$, $|f\rangle \equiv |f, m=0\rangle$ and ω_-, ω_+ are the atomic states and their eigenvalues in the magnetic field. The Hamiltonian has a symmetry with respect to a change on the direction of the magnetic field, namely, if $B \to -B$, then $|-\rangle \to |+\rangle$, $|-\rangle \to |+\rangle$ and $\omega_+ \to \omega_-$, $\omega_+ \to \omega_-$. The term coupled to an auxiliary field Ω breaks symmetry and introduces chirality in the system. Indeed, the susceptibility is given by

$$\chi_{ij}(\omega, k, B, \Omega) = \tilde{\chi}_{ij}(\omega, \Omega) + \alpha_{ijl}(\omega, \Omega)k_l + \beta_{ijl}(\omega, \Omega)B_l \tag{4.2}$$

$$+\gamma_{ijlm}(\omega, \Omega)k_l B_m, \tag{4.3}$$

where α_{ijl} describes natural optical activity and β_{ijl} describes magnetic optical activity; γ_{ijlm} describes the magnetochiral effect; ω and k are the frequency and the wave vector of the optical field. In the case of atomic vapors, γ_{ijlm} is zero. Applying an external driving field Ω leads to magneto-chirality via the last term.

1. Experimental setup

The experiment that demonstrates the symmetry breaking effect is performed in Rubidium vapor (level structure shown in Fig.39a). A schematic diagram of the

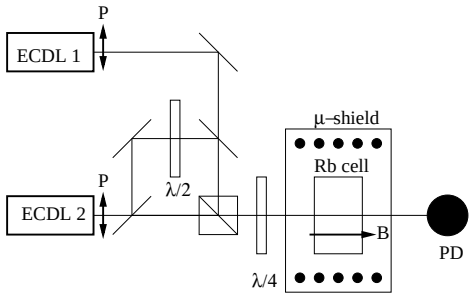

Fig. 38. Experimental setup of magnetically induced chirality

experimental setup is shown in Fig.38. Two external cavity diode lasers (ECDL) are used in our measurements. Radiation from the first ECDL used as a pump is tuned to the D_1 transition of Rb^{87} $5S_{1/2}(F = 1) - 5P_{1/2}$ $(F' = 2)$. Radiation from the second ECDL used as a probe is tuned over the transition. The linearly polarized laser beams are combined by a polarizing beam-splitter and then sent into the cell with the atomic rubidium vapor. Both beams are parallel and the diameters of the beams are the same, 1 mm. The glass cell ($l = 7.5$ cm) with atomic rubidium vapor at room temperature ($N_{Rb} \simeq 10^{10}$ cm^{-3}) is installed in a magnetic shield. A longitudinal magnetic field is created by a solenoid. The polarization of the pump field is strictly right circular. The probe field is a superposition of (uncorrelated) fields with left and right polarizations and equal optical power (the difference is less then 1%). The polarization of the probe field is not defined at any moment of time, and the probe field can be considered as an unpolarized light field. We change the time delay ($\simeq 3$ ns) between field components of the probe field with opposite polarizations, and we do not observe any influence on the recorded curves.

The typical Doppler-free resonances are shown in Fig. 40. The resonances are recorded on the transitions of Rb^{87} for different longitudinal magnetic fields. The power of the pump beam is 0.6 mW; the estimated Rabi frequency is several γ's

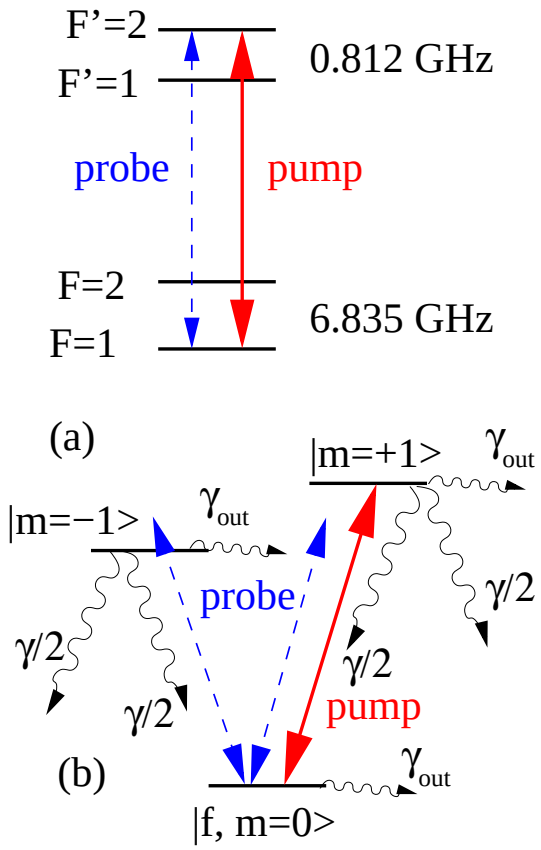

Fig. 39. (a) Rb level structure and configuration of laser fields. The pump field is circularly polarized; probe field is not polarized and can be viewed as a non–coherent mixture of left and right circular polarized light. (b) A 3-level model is used in our simulations. Relaxation of population γ is shown by undulating arrows. The simple model also accounts for flight time broadening at rate γ_{out} out of the system from all levels, and population relaxation from electronic excited states $|m = -1\rangle$ and $|m = +1\rangle$ to other than $|f, m = 0\rangle$ levels of ground state manifold via spontaneous decay. Note that for our simulation we use a simplified 3-level model; the real D1 line of Rb has three sets of similar 3-level systems: $|m = -2\rangle \leftrightarrow |f, m = -1\rangle \leftrightarrow |m = 0\rangle$, $|m = 0\rangle \leftrightarrow |f, m = +1\rangle \leftrightarrow |m = 2\rangle$, and the one shown above.

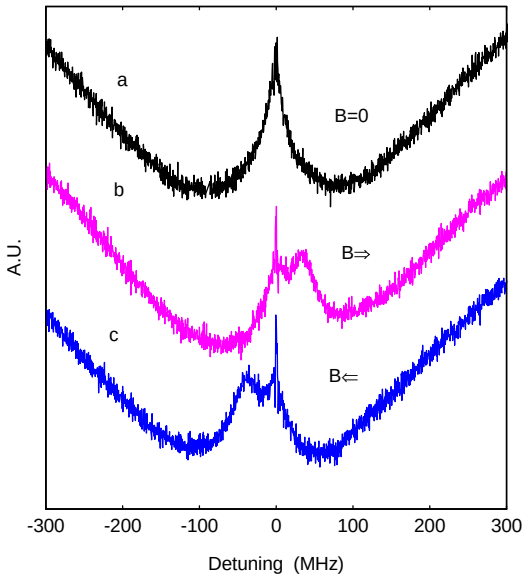

Fig. 40. Doppler-free resonances on the transition for zero magnetic field $B = 0$ (a) and opposite directions of magnetic field $B = 77$ Gauss (b and c).

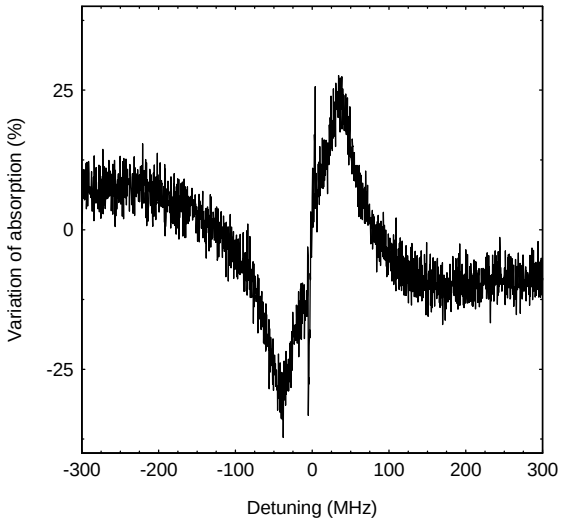

Fig. 41. Relative difference between absorption curves recorded for opposite directions of magnetic field ($B = \pm 77$ Gauss).

($\gamma = 2\pi \times 6$ MHz). This value of the Rabi frequency satisfies conditions for EIMCA in the V-scheme. The probe beam power (total) is less than 10% of the pump beam.

The transition is chosen because the effect is most pronounced in this case. In the linear regime of propagation, the laser light intensity is very small, and the probe transmission on the transition frequency is near 0.9. Nonlinear variation of absorption induced by the pump beam is near 30% of linear resonance absorption.

Note that it is difficult to define the real amplitude of Doppler-free resonance at zero detuning. Doppler free resonance on the transition has an additional narrow structure in the center. This narrow structure results from two contributions: one signal is a beat note between the pump and probe fields, and another signal is the EIT narrow resonance due to ground state coherence. (Beat note at zero frequency difference and dark resonance overlap).

2. Analysis

The first curve (Fig. 40 curve a) is the resonance on the transition at zero magnetic field, $B = 0$. The other two curves (Fig. 40 curve b) and (Fig. 40 curve c) are recorded for positive and negative longitudinal magnetic field $B = 77$ Gauss (corresponding current is $I = 1.4$ A, magnetic field B is related to current I by $B = kI$, where $k = 55$ G/A). Sharp narrow resonances which are combinations of the dark resonance and beat note indicate zero frequency difference between the pump and probe fields. It is to be noted that the pump laser frequency is tuned to the maximum of linear absorption. One can see that absorption spectra are very different for positive and negative magnetic field. There is an asymmetry in the absorption coefficient of the resonant atomic medium induced by a circular polarized pump beam.

In Figure 41, the frequency dependence of absorption difference for opposite magnetic field is presented (the result of subtraction of curves (b) and (c) shown in

previous Fig. 40 normalized to linear absorption). To the best of our knowledge, it is the largest EIMCA which has been experimentally observed. Our finding of the giant magneto-chiral anisotropy is related to the allowed electric dipole moments of resonance transitions in atoms. For a fixed laser intensity we also studied the dependence of the asymmetry on the magnetic field. The experimentally observed absorption difference as a function of the magnetic field is presented in Fig. 42. One can see that for small magnetic fields the asymmetry increases for a range of magnetic fields (where Zeeman splitting is comparable to the resonance width). Once the magnetic field is strong enough to separate resonances, the asymmetry saturates and does not depend on the magnitude of the magnetic field. We observed that above 0.6 mW of laser pump power the asymmetry changes very little. At 2.4 mW maximal symmetry is just near 30%.

As one can see, the observed asymmetry is very strong. The effect originates from the different interaction between different polarizations of unpolarized laser light and atomic levels. It can be viewed that one polarization of the probe laser interacts with a different magnetic level of the excited state than the driving laser, forming the so-called V-type configuration of atomic levels. For this component the EIT conditions can be satisfied, and it travels through the medium without absorption. Meanwhile, the orthogonal polarization of the weak probe field interacts with the same excited level as the driving field does, so the probe field experience less absorption because of saturation of the transition by the driving field. These two mechanism are different and they create substantially different responses for different polarizations, leading to chirality.

To answer the question of whether the asymmetry observed in the experiment is close to the maximal theoretical limit, we perform numerical simulations of the

self-consistent set of density matrix and Maxwell equations given by

$$\frac{\partial \rho}{\partial \tau} = -\frac{i}{\hbar}[H, \rho] - \frac{1}{2}(\Gamma\rho + \rho\Gamma), \quad \frac{\partial \Omega_{ij}}{\partial z} = -i\eta\rho_{ij}(z, \tau), \tag{4.4}$$

where Γ is the decay operator, and ρ is the atomic density matrix; Ω_{ij} is the Rabi frequency of the field frequency ν which is coupled to the transition $i \leftrightarrow j$; ρ_{ij} and $\wp_{ij}$ are the coherence and the dipole moment between levels i and j correspondingly; $\eta = \nu N \wp_{ij}/(2\epsilon_0 c)$; N is the atomic density; ϵ_0 is the permittivity of the vacuum; c is the speed of light in vacuum. It is instructive to analyze $\chi(\omega) = \eta\gamma(\omega - i\gamma)/[(\gamma + i\omega)(\gamma + ikv + i\omega) + |\Omega|^2]$, where $\omega = \omega_{+f} + gB - \nu$; γ is the relaxation rates for optical coherence. $\chi'' = \frac{\eta\gamma^2}{|\Omega|^2} + \frac{3\eta\gamma^2\omega^2}{|\Omega|^4} + \frac{2\eta\gamma^2\omega kv}{|\Omega|^4}$ where one can see that it is the spatial dispersion term kv (Doppler shift due to atomic motion) that leads to magneto-chirality in Rb vapor.

We have performed theoretical simulations by using the experimental parameters, and the results of simulations are presented in Fig. 42, where the dependence on magnetic field is shown. One can see a good agreement between the simulation and the experiment. The calculated asymmetry is higher for smaller magnetic fields because Rb atom has more levels (three sets of of V-schemes originated from the sublevels of the ground state $F = 1, m = 0, \pm 1$).

There are various applications of the obtained results ranging from optics to chemistry and biology. For example, the effect of large chirality can be used to create an optically non-isotropic environment which results in different rates of chemical photo reactions with different enantiomers.

In summary, we have implemented optically induced chirality in the Rb vapor cell. The observed anisotropy is huge. It is about 30%, and one has the possibility of creating a chiral environment for optical control of chemical reactions involving one type of enanotiomer. Another interesting possibility is to observe an inverse effect to

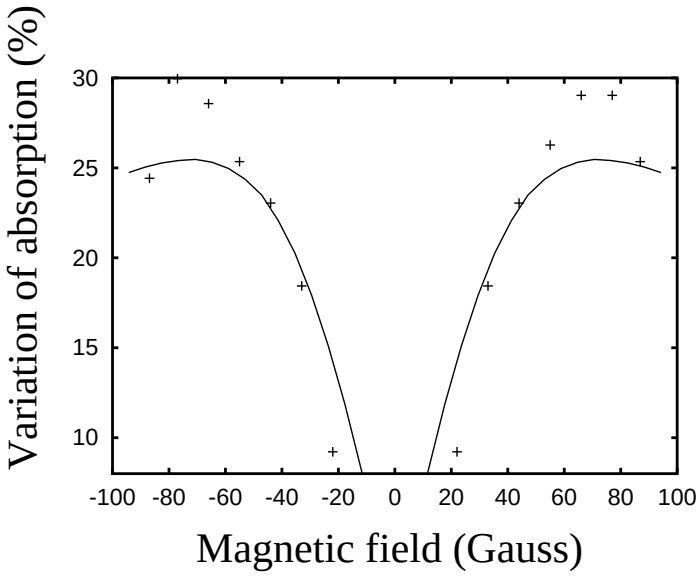

Fig. 42. Crosses dots: the laser light induced variation of absorption versus magnetic field. Solid line: the calculated laser induced relative variation of absorption versus magnetic field.

the one demonstrated here.

CHAPTER V

CONCLUSION

Let us summarize now the results obtained in the dissertation.

It has been show in the present work that atomic coherence have considerable impacts on the absorptive and dispersive properties of optical media, one can achieve Doppler-free high resolution spectroscopy via atomic coherence and quantum interference in coherently prepared media. That promises to open a new avenue to manipulate the optical property of medium quantum mechanically.

The main results in this study can be summarized as follows: In the high resolution optical spectrum experiment of Rubidium diatomic molecule, we have measured well-resolved rotational spectral components in rubidium diatomic molecules using a tunable diode laser. Wavelengths of several rotational components were measured with good accuracy using a wavemeter. The vibrational structure of the ground state is well resolved by the laser-induced fluorescence technique. Fluorescence is observed in the red wing of the band where molecular absorption is small. This indicates that an optically pumped rubidium molecular laser may be realized in these spectral regions.

With the knowledge of the transmission and fluorescence spectra, further study of many coherent effects in Rubidium diatomic molecules, such as EIT, STIRAP and FAST CARS may be possible.

Based on the spectroscopic knowledge of Rubidium diatomic molecule, , we did the Raman gain in the backward direction in rubidium diatomic molecules experiment. In this experiment, we succussed to observe the signal of Raman gain in the backward direction of probe laser. We have performed simulations that support this interpretation. Note here that what lasing in diatomic molecules via optically pumped

population inversion in the excited electronic states has previously been demonstrated in other diatomic molecules.

Cesium diatomic molecule has similar electronic, vibrational and rotational energy levels with different transition frequency.

The cesium molecular absorption transition lines in the band $B_1\Pi_u \leftarrow X_1\Sigma_g^+$ can be considered as frequency references. The sub-Doppler absorption resonances in the another cesium band $A^1\Pi_u \leftarrow X^1\Sigma_g^+$ are used for frequency stabilization of diode lasers (1083 nm)16 and Nd:YAG lasers (1064 nm)17. The Nd:YAG laser frequency stability was reached a minimum 1.310^{-11} for a measurement time of 20 s17. These results support our proposal to use the absorption lines in the shorter wavelength band $B^1\Pi_u \leftarrow X^1\Sigma_g^+$for frequency stabilization of frequency-doubled communication lasers in the spectral window around 1550 nm. Also the observation of ground state optical pumping in cesium molecular vapor shows that it is possible to observe electromagnetically induced transparency (EIT) in a Λ levels scheme in diatomic molecules. Recently EIT was observed in cascade systems in Li_2 and K_2 molecules. It opens the way to realize the quantum state memory of light in a molecular gas.

In the electromagnetically induced transparency experiment, we have experimentally observed EIT in cesium molecular gaseous medium.

With the same drive laser frequency, we observed two kinds of transmission increasing peak, the narrower one is due to Λ type transition, and the broader one is due to V type transition.

The narrow EIT peak width is much smaller than the natural linewidth of the linear transition(single photon transition), which also confirms that the two lower states of Λ type transition belong to the ground states.

The extrapolated curve of the width intersect with y axis at 1.7MHz, subtracting the two laser width 0.7 MHz, there is still 1 MHz left. Time of flight is around

$6 \times 10^{-6} s$, it gives width of 0.17MHz. The additional width is probably due to rotational relaxation of ground states.

From the experiment of electromagnetically induced transparency, we found the EIT width is less than 2 MHz. The corresponding lifetime of ground state coherence is greater than 80 nanosecond. In the allowed time region, we have observed the retrieved pulse in the same direction and with the same polarization of the signal pulse.

For diatomic molecule as Cesium dimer, at our working temperature, the most populated rotational quantum number is around 120. We work with circular polarized light of same frequency, therefore we work on the rotational sublevels of Cesium molecule.

In the atomic system there are also a lot of interesting effects of quantum optics. Magnetic induced chirality is a very novel one. we have implemented optically induced chirality in the Rb vapor cell. The observed anisotropy is huge. It is about 30%, and one has the possibility of creating a chiral environment for optical control of chemical reactions involving one type of enanotiomer. Another interesting possibility is to observe an inverse effect to the one demonstrated here.

REFERENCES

[1] M. O. Scully and M. S. Zubairy, *Quantum Optics* (Cambridge University Press, Cambridge UK, 1997).

[2] W. Hanle, Z. Phys. **30**, 93 (1924).

[3] S. H. Autler and C. H. Townes, Phys. Rev. **100**, 703 (1955).

[4] U. Fano, Phys. Rev. **124**, 1866 (1961).

[5] B. R. Mollow, Phys. Rev. **188**, 1969 (1969).

[6] C. Y. Ye, V. A. Sautenkov, T. V. Rostovtsev, G. R. Welch, and M. O. Scully, J. of Modern Optics **51**, 2555 (2004).

[7] S. Harris, Physics Today **50**, 36 (1997).

[8] V. A. Sautenkov, C. Y. Ye, Y. V. Rostovtsev, G. R. Welch, and M. O. Scully, Phys. Rev. A **70**, 33406 (2004).

[9] M. O. Scully and G. R. Welch, Physics World **17**, 31 (2004).

[10] G. L. J. A. Rikken and E. Raupach, Nature **390**, 493 (1997).

[11] G. S. Agarwal and S. Dasgupta, Phys. Rev. A **67**, 23814 (2003).

[12] V. A. Sautenkov, Y. V. Rostovtsev, H. Chen, P. Hsu, G. S. Agarwal, and M. O. Scully, Phys. Rev. Lett. **94**, 233601 (2005).

[13] P. Kusch, Phys. Rev. **49**, 218 (1936).

[14] R. Gupta, W. Happer, J. Wagner, and E. Wennmyr, J. of Chem. Phys. **68**, 799 (1978).

[15] C. D. Caldwell, F. Engelke, and H. Hage, Chem. Phys. **54**, 21 (1980).

[16] M. Mcclinto and L. C. Balling, J. of Quantitative Spectroscopy& Radiative Transfer **9**, 1209 (1969).

[17] C. Amiot, P. Crozet, and J. Vergès, Chem. Phys. Lett. **121**, 390 (1985).

[18] C. Amiot, J. of Chem. Phys. **93**, 8591 (1990).

[19] W. Demtröder, *Laser Spectroscopy* 3rd edition (Springer Verlag, Berlin Heigelberg New York 2002).

[20] M. A. Henesian, R. L. Herbst, and R. L. Byer, J. Appl. Phys. **47**, 1515 (1976).

[21] M. O. Scully, G. W. Kattawar, R. P. Lucht, T. Opatrny, H. Pilloff, A. Rebane, A. V. Sokolov, and M. S. Zubairy, Proc. Natl. Acad. Sci. USA **99**, 10994 (2002).

[22] B. Glushko, B. Kryzhanovskij, and D. Sarkisyan, Phys. Rev. Lett. **71**, 243 (1993).

[23] G. Herzberg, *Molecular Spectra and Molecular Structure: Spectra of Diatomic Molecules* (Krieger Publishing Company, New York, Van Nostrand 1989).

[24] B. Wellegehausen and H. Heitmann, Appl. Phys. Lett. **34**, 44 (1979).

[25] P. Tian, D. Keusters, Y. Suzaki, and W. S. Warren, Science **300**, 1553 (2003).

[26] D. H. Ellison, *Handbook of Chemical and Biological Warfare Agents* (CRC Press, Boca Raton FL, 2000).

[27] V. Kocharovsky, S. Cameron, K. Lehmann, R. Lucht, R. Miles, Y. Rostovtsev, W. Warren, G. R. Welch, and M. O. Scully, Proc. Natl. Acad. Sci. USA **102**, 7806 (2005).

[28] R. Bonifacio, F. A. Hopf, P. Meystre, and M. O. Scully, Phys. Rev. A **12**, 2568 (1975).

[29] V. V. Kocharovsky and V. V. Kocharovsky, Sov. Phys. Usp. **32**, 835 (1989).

[30] K. Sentrayan, A. Michael, and V. Kushawaha, Appl. Opt. **32**, 930 (1993).

[31] Y. S. Choi, Appl. Opt. **40**, 1925 (2001).

[32] M. Maier, W. Kaiser, and J. A. Giordmai, Phys. Rev. **177**, 580 (1969).

[33] H. Chen, V. A. Sautenkov,P. S. Hsu, G. R. Welch, Y. V. Rostovtsev, and M. O. Scully J. Mod. Opt. **52**, 2373 (2005).

[34] P. Kusch, Phys. Rev. **49**, 0218 (1936).

[35] B. Wellegehausen, IEEE J. of Quantum Electronics **15**, 1108 (1979).

[36] C. N. Manpichot and A. Brillet, IEEE J. of Quantum Electronics **16**, 1103 (1980).

[37] D. Sarkisyan, U. Hinze, L. Meyer, and B. Wellegehausen, Appl. Phys. B-Lasers and Optics **70**, 351 (2000).

[38] J. S. Ozcomert and P. L. Jones, Chem. Phys. Lett. **169**, 1 (1990).

[39] B. K. Clark, K. A. Page, and C. A. Stack, Chem. Phys. **163**, 371 (1992).

[40] F. W. Loomis and P. Kusch, Phys. Rev. **46**, 0292 (1934).

[41] O. A. Kocharovskaya and Y. I. Khanin, Jetp. Letters **48**, 630 (1988).

[42] M. D. Lukin, M. Fleischhauer, A. S. Zibrov, H. G. Robinson, V. L. Velichansky, L. Hollberg, and M. O. Scully, Phys. Rev. Lett. **79**, 2959 (1997).

[43] S. Brandt, A. Nagel, R. Wynands, and D. Meschede, Phys. Rev. A **56**, 1063 (1997).

[44] S. Knappe, V. Shah, P. D. Schwindt, L. Hollberg, J. Kitching, L. A. Liew, and J. Moreland, Appl. Phys. Lett. **85**, 1460 (2004).

[45] S. E. Harris and L. V. Hau, Phys. Rev. Lett. **82**, 4611 (1999).

[46] S. E. Harris and Y. Yamamoto, Phys. Rev. Lett. **81**, 3611 (1998).

[47] A. Imamoglu, H. Schmidt, G. Woods, and M. Deutsch, Phys. Rev. Lett. **79**, 1467 (1997).

[48] M. Jain, G. Y. Yin, J. E. Field, and S. E. Harris, Opt. Lett. **18**, 998 (1993).

[49] H. Schmidt and A. Imamoglu, Opt. Lett. **21**, 1936 (1996).

[50] C. Affolderbach, M. Stahler, S. Knappe, R. Wynands, G. Alzetta, A. Gozzini, L. Moi, and G. Orriols, Appl. Phys. B-Lasers and Optics **36**, 5 (1976).

[51] S. Brattke, U. Kallmann, and W. D. Hartmann, European Physical J. D **3**, 159 (1998).

[52] J. Qi, F. C. Spano, T. Kirova, A. Lazoudis, J. Magnes, L. Li, L. M. Narducci, R. W. Field, and A. M. Lyyra, Phys. Rev. Lett. **88**, 173003 (2002).

[53] J. B. Qi and A. M. Lyyra, Phys. Rev. A **73**, 043810 (2006).

[54] S. E. Harris, Phys. Rev. Lett. **70**, 552 (1993).

[55] A. S. Zibrov, M. D. Lukin, L. Hollberg, D. E. Nikonov, M. O. Scully, H. G. Robinson, and V. L. Velichansky, Phys. Rev. Lett. **76**, 3935 (1996).

[56] S. E. Harris and A. V. Sokolov, Phys. Rev. Lett. **81**, 2894 (1998).

[57] J. Kitching and L. Hollberg, Phys. Rev. A **59**, 4685 (1999).

[58] C. J. Wei and N. B. Manson, Phys. Rev. A **60**, 2540 (1999).

[59] R. Coussement, Y. Rostovtsev, J. Odeurs, G. Neyens, H. Muramatsu, S. Gheysen, R. Callens, K. Vyvey, G. Kozyreff, P. Mandel, R. Shakhmuratov, and O. Kocharovskaya, Phys. Rev. Lett. **89**, 107601 (2002).

[60] S. P. Tewari and G. S. Agarwal, Phys. Rev. Lett. **56**, 1811 (1986).

[61] S. E. Harris, G. Y. Yin, M. Jain, H. Xia, and A. J. Merriam, Philosophical Transactions of the Royal Society of London Series a-Mathematical Physical and Engineering Sciences **355**, 2291 (1997).

[62] K. Hakuta, L. Marmet, and B. P. Stoicheff, Phys. Rev. A **45**, 5152 (1992).

[63] A. B. Matsko, O. Kocharovskaya, Y. Rostovtsev, G. R. Welch, A. S. Zibrov, and M. O. Scully, Advances in Atomic, Molecular, and Optical Physics, **46**, 191 (2001).

[64] S. E. Harris and Y. Yamamoto, Phys. Rev. Lett. **81**, 3611 (1998).

[65] L. V. Hau, S. E. Harris, Z. Dutton, and C. H. Behroozi, Nature **397**, 594 (1999).

[66] M. M. Kash, V. A. Sautenkov, A. S. Zibrov, L. Hollberg, G. R. Welch, M. D. Lukin, Y. Rostovtsev, E. S. Fry, and M. O. Scully, Phys. Rev. Lett. **82**, 5229 (1999).

[67] D. Budker, D. F. Kimball, S. M. Rochester, and V. V. Yashchuk, Phys. Rev. Lett. **83**, 1767 (1999).

[68] M. Bajcsy, A. S. Zibrov, and M. D. Lukin, Nature **426**, 638 (2003).

[69] A. S. Zibrov, A. B. Matsko, O. Kocharovskaya, Y. V. Rostovtsev, G. R. Welch, and M. O. Scully, Phys. Rev. Lett. **88**, 103601 (2002).

[70] L. D. Landau and E. M. Lifshitz, *Electrodynamics of Continuous Media* (Pergamon, Oxford, 1984).

[71] V. A. Markelov, M. A. Novikov, and A. A. Turkin, JETP Letters **25**, 378 (1977).

[72] N. G. Kalugin, P. Kleindienst, and G. H. Wagniere, Chem. Phys. **248**, 105 (1999).

[73] L. D. Barron, Nature **405**, 895 (2000).

[74] L. D. Barron and J. Vrbancich, Molecular Physics **51**, 715 (1984).

[75] N. B. Baranova and B. Y. Zeldovich, Molecular Physics **38**, 1085 (1979).

[76] M. Vallet, R. Ghosh, A. Le Floch, T. Ruchon, F. Bretenaker, and J. Y. Thepot, Phys. Rev. Lett. **8718**, 183003 (2001).

[77] S. Wielandy and A. L. Gaeta, Phys. Rev. Lett. **81**, 3359 (1998).

VITA

Name: Hui Chen

Address:
Department of Physics,
Texas A&M University,
College Station, Texas 77843-4242,
Phone: 979-458-1528, 979-458-1136,
Fax: 979-845-1235,
e-mail: huichen@physics.tamu.edu

Education

M.S. Degree in Physics, May, 2004.
Texas A&M University, College Station,TX, US

M.S. Degree in Physics, July, 2001.
University of Science and Technology of China, Hefei, Anhui, China

B.S. Degree in Physics, July, 1998.
University of Science and Technology of China, Hefei, Anhui, China

Experience

2001-2006

Research and Teaching Assistant at Department of Physics, Texas A&M University

1998-2001

Research and Teaching Assistant at Department of Physics, University of Science and Technology of China, Hefei, Anhui, China

Publications

1. V. A. Sautenkov, Y. V. Rostovtsev, H. Chen, P. Hsu, Girish S. Agarwal, and M.O. Scully Physical Review Letters **94**, 233601 (2005).

2. Hui Chen, Vladimir A. Sautenkov, Paul S. Hsu, George R. Welch, Yuri Rostovtsev and Marlan O. Scully Journal of Modern Optics **52**, 2373 (2005).

3. Hui Chen, Hebin Li, Yuri Rostovtsev, Mikhail A. Gubin, Vladimir A. Sautenkov and Marlan O. Scully J. Opt. Soc. Am. B **23**, 723 (2006).

4. Hui Chen, Zoe-Elizabeth Sariyanni, Vladimir A. Sautenkov, Yuri Rostovtsev and Marlan O. Scully Accepted Journal of Modern Optics (2006).

5. Hui Chen, Hebin Li, Vladimir A. Sautenkov, Yuri Rostovtsev and Marlan O. Scully In preparation (2006).

6. Hebin Li, Hui Chen, Yuri Rostovtsev, Vladimir A. Sautenkov and Marlan O. Scully Submitted to Optics Communication (2006).